SYNTHESIS AND CHARACTERIZATION OF CLAY-SUPPORTED NANOPARTICLES OF ZERO-VALENT IRON AND ITS APPLICATION FOR THE REMOVAL OF AQUEOUS Co^{2+} AND Cu^{2+} IONS

A Thesis Submitted to
the Graduate School of Engineering and Science of
İzmir Institute of Technology
in Partial Fulfillment of the Requirements for the Degree of

MASTER OF SCIENCE

in Chemistry

by
Çağrı ÜZÜM

December 2007
İZMİR

We approve the thesis of **Çağrı ÜZÜM**

Assoc. Prof. Dr. Talal SHAHWAN
Supervisor

Prof. Dr. Ahmet E. EROĞLU
Co-Supervisor

Prof. Dr. Çetin GÜLER
Committee Member

Assoc. Prof. Dr. Sedat AKKURT
Committee Member

Assoc. Prof. Dr. Hürriyet POLAT
Committee Member

17 December 2007

Date

Prof. Dr. Levent ARTOK
Head of the Chemistry Department

Prof. Dr. Hasan Böke
Dean of the Graduate School of
Engineering and Sciences

ACKNOWLEDGEMENTS

I would like to thank my supervisor Assoc. Prof. Dr. Talal R. A. SHAHWAN, for his farseeing guidance, endless support and generous help throughout this thesis study.

I would also like to thank my co-supervisor Prof. Dr. Ahmet E. EROĞLU for his valuable suggestions and kind helps.

Special thanks to group members of Materials Research Center, Evrim YAKUT, Mine BAHÇECİ, Duygu OĞUZ, and Gökhan ERDOĞAN for their helps in XRD, SEM and BET analyses. I would like to thank Dr. Sinan YILMAZ at İYTE Department of Chemistry, for his helps in AAS analysis. For TEM and EELS analyses, I owe my thanks to Dr. Ingo Lieberwirth at Max Planck Institute for Polymer Research, Mainz and thanks to Dr. Tom B. Scott and Dr. Keith R. Hallam at Interface Analysis Center, Bristol University for XPS analyses.

Also, I would like to thank Özge TUNUSOĞLU and Nazlı EFECAN, for their kindness during my laboratory studies and my friends at İYTE Department of Chemistry for their sincere helps.

For the funding, I am pleased to pay my thanks to Rectorship of İYTE for this thesis was a part of an İYTE Scientific Research Project (2006 BAP 13).

Finally, I would like to express my endless thanks to my beloved family for their motivation and continuous support.

ABSTRACT

SYNTHESIS AND CHARACTERIZATION OF CLAY-SUPPORTED NANOPARTICLES OF ZERO-VALENT IRON AND ITS APPLICATION FOR THE REMOVAL OF AQUEOUS Co^{2+} AND Cu^{2+} IONS

In recent years Permeable Reactive Barriers (PRBs) are being developed and used in the removal of organic and inorganic pollutants from surface water and groundwater. Zero-valent iron is viewed as an ideal reactive material for PRBs by means of its high sorption/reduction capacity towards various toxic ions. Zero-valent iron synthesized in nanoscale has a greater affinity to reduce/adsorb various toxic aqueous ions by virtue of its large surface area**.**

In this work, nanoscaled (10-100nm) zero-valent iron (nZVI) was synthesized in ethanol by borohydride reduction method in atmospheric conditions. It was observed that iron nanoparticles are mainly in zero-valent oxidation state and that they remain without significant oxidation for weeks. To enhance its effect and usability, nZVI was supported by kaolinite and montmorillonite during synthesis. Characterization of those clay-supported nZVI was performed using XRD, SEM, TEM, EELS, XPS, Zeta Meter, BET-N_2. Iron nanoparticles consist of a zero-valent core and a surrounding oxide shell with approximate thickness of 3-5 nm. The application of clays as support materials have led to a partial decrease in the aggregation of iron nanoparticles known to normally form chain-like structure. The diameter of unsupported iron nanoparticles was predominently within the range 20-80 nm, while clay-supported iron nanoparticles existing as dispersed nano spheres had particle diameters within 10-50 nm.

The synthesized materials were applied as adsorbents for Co^{2+} and Cu^{2+} ions. According to the results , unsupported and clay-supported nZVI has a great capacity to immobilize Co^{2+} and Cu^{2+} ions with very fast kinetics. While Co^{2+} seems to be fixed via the oxohydroxyl groups on the surface of iron nanoparticles, Cu^{2+} was fixed by a redox mechanism that lead to formation of Cu_2O and Cu^0. The performed studies indicate that kaolinite- and montmorillonite-supported zero-valent iron nanoparticles are promising reactive materials for environmental applications.

ÖZET

KİL DESTEKLİ SIFIR DEĞERLİKLİ DEMİR NANOTANECİKLERİNİN SENTEZİ, KARAKTERİZASYONU VE SUDAKİ Co^{2+} VE Cu^{2+} İYONLARININ UZAKLAŞTIRILMASI AMAÇLI UYGULAMASI

Geçirgen reaktif bariyer teknolojisi son yıllarda yüzey ve yeraltı sularındaki toksik iyonların uzaklaştırılmasında kullanılan geleneksel yöntemlere alternatif olarak geliştirilip kullanılmaktadır. Sıfır değerlikli demir, bir çok toksik iyonu tutma/indirgeme kapasitesinden dolayı, geçirgen bariyerler için ideal bir reaktif maddedir. Sıfır değerlikli demir nano boyutlarda sentezlenirse daha geniş yüzey alanına ve etkiye sahip olur.

Bu çalışmada, nanoboyutlu (10-100nm) demir parçacıklarının sentezi, atmosferik koşullarda, etanol içinde borhidrür indirgemesiyle gerçekleştirilmiştir. Elde edilen taneciklerin temel olarak sıfır-değerlikli demirden oluştuğu ve bu formunu büyük ölçüde haftalarca koruduğu gözlenmiştir. Etkisinin ve kullanılabilirliğinin artırılması amacıyla, sıfır değerlikli demir nanotnacikleri (SDDN), kaolinit veya montmorillonit destekli olarak sentezlenip, XRD, SEM, TEM, EELS, XPS, Zetametre, BET-N_2 yüzey alanı metotları kullanılarak karakterize edilmiştir. Demir nanotaneciklerinin sıfır-değerlikli çekirdek ile 3-5 nm kalınlığında demir oksit kabuğundan oluştuğu gözlenmiştir. Destek maddesi olarak killerin kullanılması normalde zincirsi yapılar oluşturan demir nanotaneciklerinin kısmen dağılmasını sağlamıştır. Desteksiz SDDN 20-80 nm kalınlığında zincirsi yapılar oluştururken, kil-destekli SDDN'nin çoğunlukla 10-50 nm çapında ayrı kürecikler halinde bulunduğu gözlenmişir.

Sentezlenen maddeler Co^{2+} ve Cu^{2+} iyonlarının sudan arındırılmasında kullanılmış, maddelerin bu iyonlara karşı yüksek ve kinetik olarak hızlı tutma kapasitesine sahip olduğu gözlenmiştir. Co^{2+} demir yüzeyindeki oksohidroksil gruplarına tutunurken, Cu^{2+} indirgenme-yükseltgenmeye dayalı olarak Cu_2O ve Cu^0 formlarına döünsmüştür. Bu sonuçlara göre kaolinit- ve montmorillonit-destekli demir nanotanecikleri çevre uygulamalarında önemli bir rol oynamaya adaydır.

To my sister, mother and father...

TABLE OF CONTENTS

LIST OF FIGURES

LIST OF TABLES

CHAPTER 1

INTRODUCTION

1.1. Heavy Metal Pollution in Aqueous Media

The pollution in natural and waste waters is a major environmental problem in the modern world. Pollution can be caused by heavy metals as well as organic chemicals (e.g. halogenated hydrocarbons, benzene, toluene, etc.) and other inorganic species (e.g. nitrate ion, phosphate ion, etc.).

Heavy metals are a group of elements between copper and bismuth on the periodic table and they have specific gravities greater than 4.0. Even though trace amounts of some heavy metals, including iron, cobalt, copper, manganese, molybdenum, vanadium, strontium, and zinc are necessary for life, greater levels can be harmful to organisms and can cause death. The sources of heavy metals in the body are air, food and drinking water. Since heavy metal poisoning by food chain is also closely related to contamination in natural waters, effective remediation of polluted water is essential for health. This study focuses on the stabilization of two specific heavy metals in aqueous media; cobalt and copper.

Copper is mostly used in the production of wires throughout the electrical industry, armature windings, water pipes, pigments, chemical equipment and it is one of the mostly used metals by mankind (Scheinberg 1991). Also, copper salts exist in fungicides and algaecides. Sources of copper contamination in natural aqueous media may be mining, metal plating, domestic and industrial wastes (Manahan 1991, Evangelou 1998). Maximum contamination level (MCL) is 1.9 mg L^{-1} according to U.S. Public Health Service (USPHS) but the contamination is mostly in the levels of 20 μg/L (Pagenkopf 1978). The most stable copper ion is in divalent form but under special conditions both +1 and +3 states can occur. Too much copper in the body can inhibit the enzyme dihydrophil hydratase, an enzyme involved in haemopoiesis. An inherited condition called Wilson's disease causes the body to retain copper, since it is not excreted by the liver into the bile. If this disease is not treated, brain and liver damage can occur. Too much copper in water has also been found to damage marine life. The

observed effect of these higher concentrations on fish and other creatures is damage to gills, liver, kidneys, and the nervous system (Wikipedia 2007a).

Cobalt exists in the principal minerals smaltite ($CoAs_2$) and caboltite (CoAsS) and it only represents the 4×10^{-3} percent of the earth's crust. Cobalt is commonly in two oxidation states, +2 and +3. In oxygenated waters +2 state is immediately oxidized to +3 state but since +3 state hydrolyzes, its observed concentrations are low (Pagenkopf, 1978). Among 22 radioisotopes of cobalt, only one isotope is stable: ^{59}Co. Most stable radioactive isotope is ^{60}Co with a half-life of 5.2714 years. Cobalt is used in the preparation of magnetic, wear-resistant, and high-strength alloys. Its compounds are used in ink, paint, and varnish industry. Small amounts of this metal are essential to many living organisms, including humans. 0.13 to 0.30 mg/kg of cobalt in soils improves the health of grazing animals. Cobalt is also a central component of the vitamin cobalamin, or vitamin B_{12} and it is only slightly toxic. The isotope ^{60}Co is commonly used in radiotherapy, sterilization of medical supplies, and medical waste. But this high-energy gamma emitting isotope can cause severe burns and death. Extended exposures increase the risk of morbidity or mortality from cancer (Wikipedia 2007b).

Until the 1980s, mankind was concerned more about the pollution in surface water (e.g. rivers, lakes, etc.), but it is now known that underground water resources are also under the threat of pollution. Another thing that is now known is that pollution in groundwater is a more serious situation for two reasons. First, groundwater is a major source of drinking water and second, remediation of groundwater is much harder and much more expensive compared to the that of surface water (Baird 2001).

Some of the techniques for remediation of both surface water and groundwater are discussed below.

1.2. Remediation of Water

Ex situ Methods: Removing the contaminant source and pump-and-treat systems are examples for *ex situ* techniques. Removing the contaminant source is not always possible for groundwater. Especially some dense organics like polychlorinated solvents are persistent in soil and slightly soluble in water, so they provide a continuous supply of contaminants to groundwater (Baird 2001, Blowes, et al. 2000).

In pump-and-treat systems, polluted water is pumped from the aquifer to an isolated container, treated here to remove organic or inorganic contaminants and then cleaned water is returned back to aquifer or transferred to another water body. Here a huge amount of water must be transferred for remediation and cost is very high. Also there are some other environmental problems during the re-introduction of treated water to aquifers like enhancing the dissolution of slightly soluble toxic materials remaining in the aquifer (Baird 2001).

In situ Methods: *In situ* remediation methods include;

(a) Direct injection of reactive materials to aquifers: In this technique, reactive materials are simply injected to the aquifer of migrating plume of groundwater and they are expected to move in the direction of migration to reach the contaminated zone. After the reactive materials reach to the contaminated zone, they react with the contaminants to destruct or stabilize them and remediate the groundwater. It is clear that reactive materials should be in contact with contaminants, so they must be highly mobile to be driven by migration.

(b) Reactive treatment zones: In this method reactive materials remediating water are added to special sites where they are expected to remain constant on the grains of native aquifer material. A low mobility of reactive materials is essential.

(c) Permeable reactive barriers (PRBs) are developed as an alternative to these classical techniques and being developed for more than 15 years. A large number of inorganic contaminants, including As, Cd, Cr, Cu, Hg, Fe, Mn, Mo, Ni, Pb, Se, Tc, U, V, NO_3, PO_4 and SO_4 were treated by this technique in laboratory scales. Also small-scale field studies have demonstrated treatment of Cd, Cr, Cu, Fe, Ni, Pb, NO_3, PO_4 and SO_4. Permeable reactive barriers can be imagined as huge horizontal columns placed in the path of a migrating plume of contaminated groundwater. Reactive materials and non-toxic filling materials (e.g. sand, clays, etc.) are embedded into these columns (barriers). Reactive materials are selected to promote geochemical reactions that result in the destruction or stabilization of the groundwater contaminants (Blowes, et al. 2000). The reactive material as well as the other parts of the setup, of course, must be less toxic than the pollutants (Nuxoll, et al. 2003).

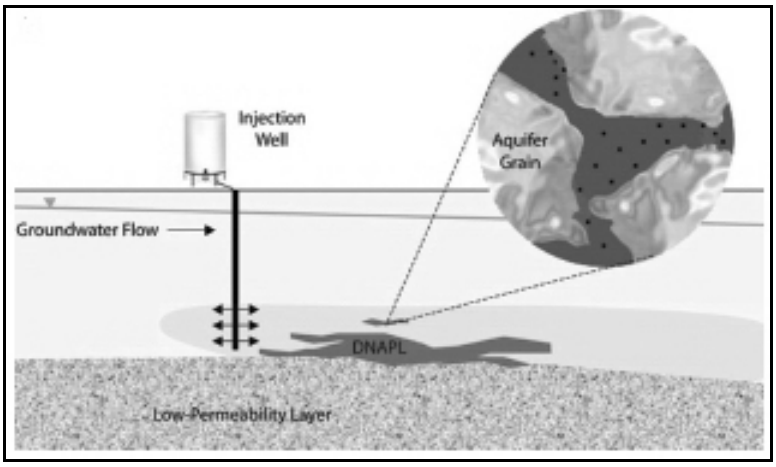

Figure 1.1. Direct injection method for remediation of groundwater
(Source: Tratnyek and Johnson 2006)

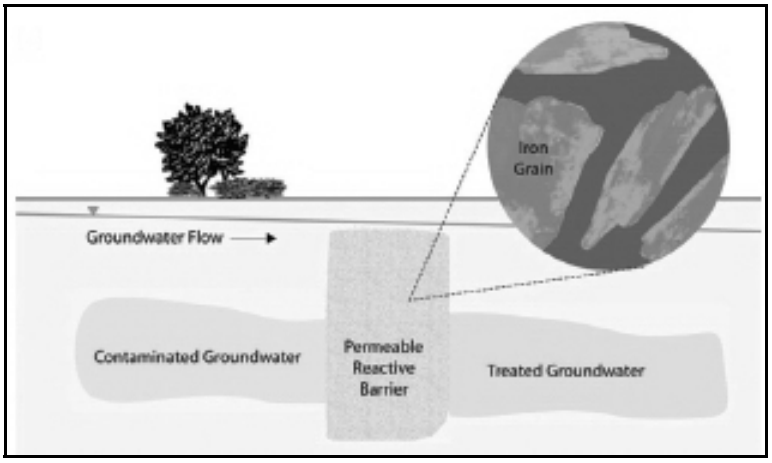

Figure 1.2. PRB application for groundwater remediation.
(Source: Tratnyek and Johnson 2006)

If a suitable reactive material is selected for PRBs, a wide range of reaction mechanisms can be employed to remove both negatively charged and positively charged inorganic species from migrating groundwater at the same time (Blowes, et al. 2000). Treatment of major hazardous organic species is also possible.

Despite some economic hurdles and some scientific gaps, recent developments demonstrate the potential of PRBs for *in situ* remediation of groundwater (Zhang and Elliot 2006).

Next section presents information about nanoscaled zero-valent iron (nZVI) which has been proposed as a reactive material for both *in situ* and *ex situ* remediation of water.

1.3. Nanoscaled Zero-Valent Iron (nZVI)

Iron, Fe, is placed in group 8 and period 4 of periodic table with atomic number 26. Iron mainly consists of four isotopes: 5.845% of radioactive ^{54}Fe with half-life: $>3.1\times10^{22}$ years, 91.754% of stable ^{56}Fe, 2.119% of stable ^{57}Fe and 0.282% of stable ^{58}Fe. Another isotope, ^{60}Fe has a half-life of 1.5 million years. Iron in elemental form is very reactive and it is immediately oxidized in atmospheric conditions. So it exists in the form of magnetite (Fe_3O_4), hematite (natural ore) (Fe_2O_3), limonite or siderite. Figure 1.3 summarizes the standard reduction potentials of iron species.

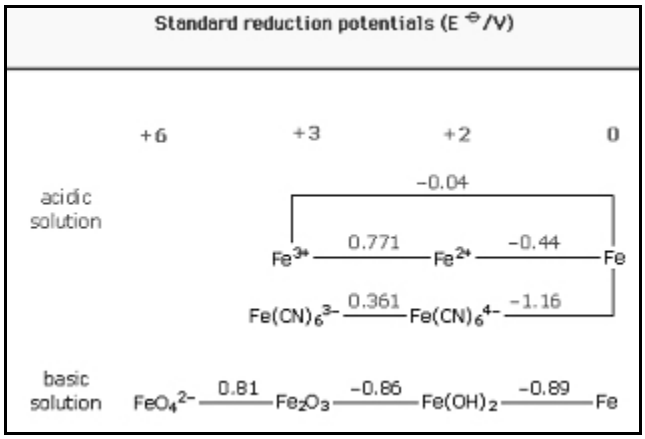

Figure 1.3. Standard reduction potentials of iron species
(Source: Web of Elements 2007)

Iron is essential for all living organisms, mainly acting as the basic component of oxygen carrier hemoglobins. Though, in excessive amounts it can be toxic, since free ferrous iron reacts with peroxides to produce free radicals, which damage several essential structures in bodies (Wikipedia 2007c). Iron has a body centered cubic structure that can be observed by the main X-ray diffraction line at about 45 2 theta

degrees. Iron is the fourth-most abundant element in the Earth's crust, it is cheap and relatively innocuous. Several studies demonstrated that zero-valent iron is effective at stabilization or destruction of a host of pollutants by its highly reducing character. From these aspects, zero-valent iron (ZVI) is proposed as one of the best reactive materials in permeable reactive barrier (PRB) technology (Çelebi, et al. 2007).

If zero-valent iron is synthesized in nanoscales, its specific surface area increases dramatically (Figure 1.4). Surface reactivity is therefore enhanced such that in comparison to 325 mesh iron powder, nanoscaled iron particles were reported to have a 30 times higher remediation rate for Cr(VI) and Pb(II) (Ponder, et al. 2000).

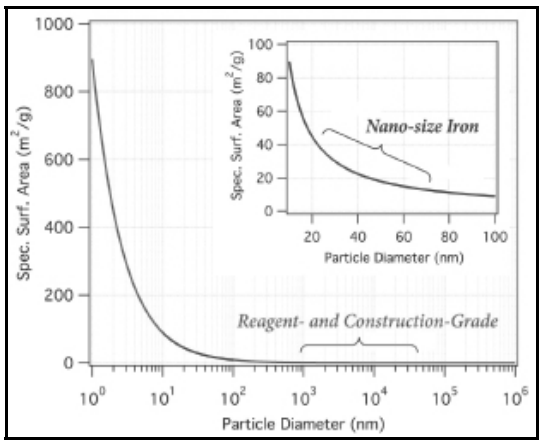

Figure 1.4. Specific Surface Area vs. Particle Diameter.
(Source: Tratnyek and Johnson 2006)

In laboratory scale, nanoscaled zero-valent iron (nZVI) was used to destruct or stabilize halogenated hydrocarbons (Wang and Zhang 1997, Zhang 2003), carbon tetrachloride (Nurmi, et al. 2005), polychlorinated biphenyls (PCBs) (Varanasi, et al. 2007), Cr(VI) and Pb(II) (Ponder, et al. 2000), As(III) (Kanel, et al. 2005), As(V) (Kanel, et al. 2006), nitrate (Wang, et al. 2006a, Sohn, et al. 2006), Ba(II) (Çelebi, et al. 2007), Ni(II) (Li and Zhang 2006) and sulfur in biosolids (Li, et al. 2007).

Nanoscaled zero-valent iron can be synthesized by several methods (Sun, et al. 2006, Nurmi, et al. 2005, Li, et al. 2006). The most widely used method for environmental purposes is the borohydrate reduction of Fe(II) or Fe(III) ions in aqueous

media. The method presented by Wang and Zhang consists of dropwise addition of sodium borohydride ($NaBH_4$) to a solution of Fe(II) or Fe(III) (Wang and Zhang 1997). One of the proposed mechanisms for the reaction is:

$$Fe^{2+} + 2BH^- + 6H_2O \rightarrow Fe^0 + 2B(OH)_3 + 7H_2 \uparrow \text{ (Wang, et al. 2006a)}$$

Synthesized zero-valent iron is unstable in atmospheric conditions and it tends to form oxides/hydroxides in the forms of Fe_2O_3, Fe_3O_4 and FeOOH (Noubactep, et al. 2005). In former studies, synthesis of nZVI and even the experiments for the adsorption of several species were performed in inert conditions to keep iron in its zero-valent form. In recent studies including this thesis work, nZVI is synthesized in open air in the presence of ethanol to prevent massive oxidation (Liu, et al. 2005a, Liu, et al. 2005b). Whatever precautions are taken to prevent oxidizing, it is observed that nZVI consists of a zero-valent core and an oxide shell (core-shell structure). For iron nanoparticles produced by the sodium borohydride reduction of iron salts, only limited information on the surface characterization has been published (Li and Zhang 2007, Sun, et al. 2006). The oxide shell has a thickness of about 5 nm and is formed of only FeOOH according to Li and Zhang (Li and Zhang 2007). On the other hand Wang, et al. stated that the surface of nZVI is mainly an iron–boron noncrystalline alloy (Wang, et al. 2006a). According to another study, boron present in the shell of iron nanoparticle is mobile and can be removed by simple washing (Nurmi, et al. 2005). Some authors claim that magnetite/maghemite ($Fe_3O_4/\gamma\text{-}Fe_2O_3$) also exist in the structure (Lien, et al. 2007, Zhang, et al. 2006). Figure 1.5 shows the core-shell structure of nZVI suggested by Li and Zhang in 2007. The authors studied nZVI structure before and after contacting with various metals and proposed three possible types of metal uptake on nZVI surface. According to this view; (i) only physical sorption occurs for cations having standard reduction potential, E^0, more negative than or close to that of Fe, (ii) both sorption and chemical reduction arises for cations having E^0 slightly more positive than that of Fe and (iii) only chemical reduction occurs for cations with E^0 higher than that of Fe. Figure 1.5 also summarizes these phenomena (Li and Zhang 2007). There are several studies that focused on the characterization and synthesis mechanisms of nZVI, but further effort is still needed to better clarify its structure.

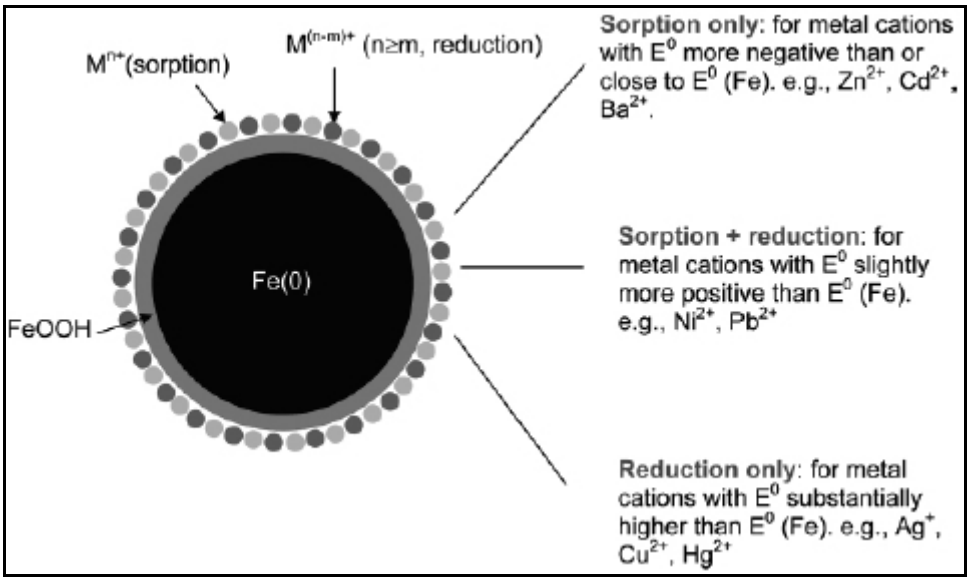

Figure 1.5. A model for core-shell structure of nZVI and metal uptake mechanisms. (Source: Li and Zhang 2007)

Despite its high chemical treating capacity, there are some restrictions on the usage of nZVI in real remediation applications. The first restriction arises in permeable reactive barrier (PRB) technology. As mentioned in section 1.2, PRBs are some huge columns placed in the path of migrating mass of water. The reactive material in PRB cannot be pure nZVI because of various reasons, the most important of which is the high costs associated with massive amount of required zero-valent iron nanoparticles. There are hurdles to surmount also from the colloidal viewpoint; iron nanoparticles have positive surface charges within the natural pH range and they tend to repel each other strongly and it is very hard to keep them stable in the permeable reactive barrier.

Second restriction arises in *in situ* applications where PRBs or special remediation sites are not used. In these kind of applications, nZVI plume is directly injected to an aquifer of groundwater and it is expected to migrate to contaminated zones (Tratnyek and Johnson 2006). A high mobility of nanoparticles is essential in direct injection applications. But due to colloidal properties of nZVI, particles tend to precipitate and they cannot be driven for more than a few meters by the migration of water and probably cannot reach the contaminated zone.

Another problem, valid for all methods, is the storage of iron nanoparticles for a long time without oxidizing since thermodynamically zero-valent iron tends to react

with oxygen. A more detailed summary of difficulties arising with the use of zero-valent iron nanoparticles is given elsewhere (Li, et al. 2006).

To overcome these problems, iron nanoparticles can be modified, supported or mixed with a filling material like sand.

1.4. Modified / Supported Nanoscaled Zero-Valent Iron

In recent years there have been attempts to increase the remediation ability of nZVI. Pd catalyzed nZVI were determined to have a higher affinity for destruction of halogenated hydrocarbons (Wang and Zhang 1997). In another study, bimetallic nanoparticles of nickel and iron were synthesized to determine the effects of a second metal on the dehalogenation of hydrocarbons and it was concluded that Ni acts as a hydrogenation catalyst in Ni-Fe nanoparticles (Schrick, et al. 2002). In another work, iron nanoparticles supported on a hydrophobic resin called PolyFlo were used to stabilize Cr(VI) and Pb(II) (Ponder, et al. 2000). There was also an attempt to control the size of zero-valent iron nanoparticles by using various types of carboxymethyl cellulose (CMC) as stabilizers (He and Zhao 2007). It is reported that the stabilizers caused a significant decrease in nanoparticle size. Zhu et al. (2006) synthesized palladized nanoscale zero-valent iron particles supported on chitosan and silica for the reductive dechlorination of 1,2,4-trichlorobenzene and observed an enhancement in reaction with increasing Pd in the sorbent. Another synthesis of supported nZVI was reported by Zhang et al. (2006). The researchers produced and used nanoscale zero-valent iron supported on exfoliated graphite for the removal of nitrate. In comparison to the great interest in synthesizing and using zero-valent iron nanoparticles for environmental purposes, very little effort was devoted to synthesizing and studying supported iron nanoparticles. In particular, the production of nZVI supported on natural minerals, like clays, has not been reported yet.

1.5. Clay Supported Nanoscaled Zero-Valent Iron

Clay minerals are basically hydrous aluminum silicates having small particle size (< 2μm). Mg and Fe may exist instead of aluminum and the clay may contain alkali or rare earth elements as constituents. A pure clay mineral consists of two basic blocks;

a sheet of silicon tetrahedrons and another sheet of aluminum octahedrons. The type of the clay minerals is determined by the stacking of these two sheets into layers, the properties of the bonding between layers and existence of different ions substituted for aluminum and silicon. Clay minerals have plasticity when wet, they are thermally / chemically stable in geochemical media in a wide range of pH in addition to their low costs and wide availability. Clays of concern in this study, kaolinite and montmorillonite, are potential heavy metal adsorbents (Shahwan 2000). These properties make clay minerals suitable filling and/or support materials for zero-valent iron nanoparticles for *in situ* remediation methods.

Kaolinite consists of a sheet of aluminum ions octahedrally coordinated and a sheet of silicon ions tetrahedrally coordinated. Kaolinite can be formulated as $Al_2Si_2O_5(OH)_4$ and nearly all minerals of the kaolinite group have this ideal composition. Kaolinite is classified as a 1:1 clay because each structural unit is formed of one octahedral and one tetrahedral sheet as shown in Figure 1.6. When these sheets come into contact with each other, OH^- ions on one sheet form hydrogen bonding with the O^{2-} layer of the neighboring sheet resulting a tightly bound structure. Kaolinite does not swell or shrink much on introducing or removing water. That is an outcome of the nonexpanding character of kaolinite, it cannot absorb water into its interlayer space. Kaolinite has a unit layer of about 7Å which can be observed from the characteristic x-ray diffraction line corresponding to about this thickness (Shahwan 2000).

Montmorillonite is a member of smectite family. It has a 2:1 layer structure in which a central octahedral sheet is placed between 2 tetrahedral sheets (Figure 1.6). Montmorillonite does not have a constant water ratio and because of weak interlayer bonds, when introduced in water, its volume increases dramatically. It is hydrated sodium calcium aluminum magnesium silicate hydroxide formulated as $Na_x\{Mg_xAl_{2-x}(OH)_2[Si_4O_{10}]\}.nH_2O$ (Wikipedia 2007d). The substitution of Mg^{2+} for Al^{3+} in octahedral sheets gives rise to a permanent negative charge which is balanced by various cations in interlayer spaces like Na^+, K^+ and Ca^{2+} (Shahwan 2000).

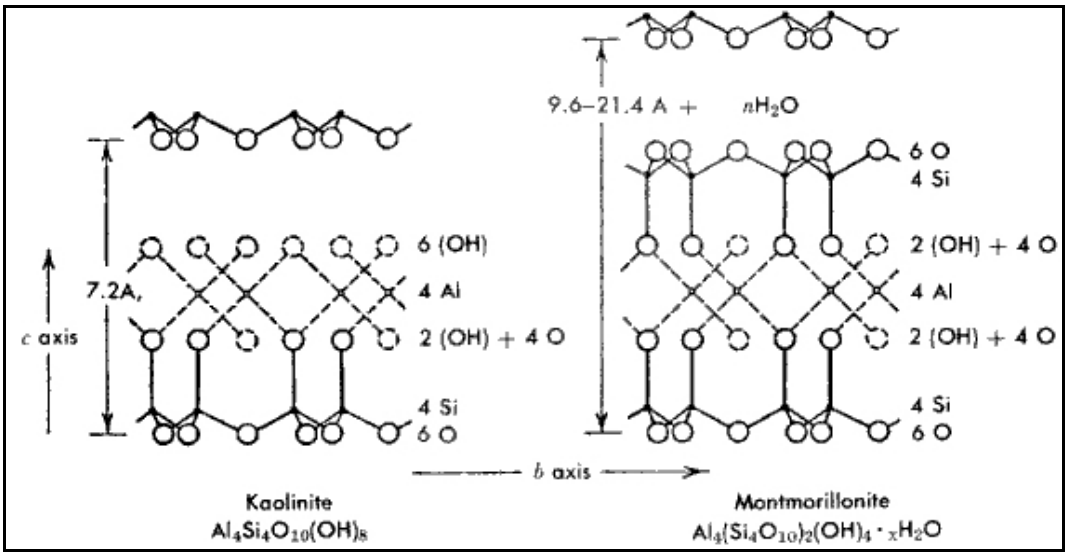

Figure 1.6. Structures of Kaolinite and Montmorillonite
(Source: Seafriends 2007)

In direct injection remediation method (section 1.2), a high mobility of nanoparticles is preferred and particles with slower precipitation rates give better results. Zero-valent iron nanoparticles are known to settle down instead of hanging in the solution so modification of iron nanoparticles by dispersing agents or support materials is a must for these kinds of applications.

In permeable reactive barriers (PRBs) (section 1.2), proposed as an *in situ* remediation technique, reactive materials -iron nanoparticles in this case- are preferred to have less repulsion between their colloidal particles so that the particles remain in the barrier rather than migrate with the plume of water. In contrary to iron nanoparticles, clay minerals like kaolinite and montmorillonite have negative surface charges in natural media and they act as electrostatic attraction matrices for nZVI. Geological stability, low costs and high availability of clay minerals are also a great advantage for big scale applications. The most important of all is the potential of kaolinite and montmorillonite for the dispersion of zero-valent iron nanoparticles. If the dispersion of nanoparticles is achieved, specific surface area and probably specific surface reactivity of nanoparticles will increase, resulting in a great enhancement in remediation capacity.

1.6. Aim of the Study

This study focuses on the synthesis of kaolinite- and montmorillonite-supported zero-valent iron nanoparticles at various clay/iron ratios and the characterization of the synthesized materials in terms of size, surface and colloidal properties. The products are then used for the removal of aqueous Co^{2+} and Cu^{2+} ions under various experimental conditions. The effects of (volume of solution)/(mass of sorbent) ratio, contact time, initial metal concentration, pH of solution and initial (clay/iron) ratio are investigated to clarify the sorption properties of clay supported iron nanoparticles against Co^{2+} and Cu^{2+}. For the characterization of synthesized clay supported nanoscaled zero-valent iron (nZVI) solids, several bulk and surface techniques are used. To characterize the crystallographic structure, X-ray Powder Diffraction (Powder XRD) is used. Images in nanoscales are recorded by Scanning Electron Microscopy (SEM) and Transmission Electron Microscopy (TEM). Energy Dispersive X-ray Spectroscopy (EDS) technique is applied to determine the quantitative distribution of elements on the surfaces and the oxidation states of surface species are analyzed by X-ray Photoelectron Spectroscopy (XPS). Also mapping of elements on the surfaces are recorded by EDS and Electron Energy Loss Spectroscopy (EELS). Atomic Absorption Spectrometry (AAS) analysis is performed to determine the aqueous concentrations of Co^{2+} and Cu^{2+} species.

CHAPTER 2

EXPERIMENTAL

2.1. Chemicals and Reagents

Throughout this study $FeCl_2$. $4H_2O$ (Sigma-Aldrich 22029-9), $NaBH_4$ (Aldrich 4511-2), kaolinite (Fluka 03584), montmorillonite K-10 (Aldrich 28152), absolute ethanol (Riedel-de Haën 32221), $CoCl_2$. $6H_2O$ (Riedel-de Haën 31277) and $Cu(NO_3)_2$. $2.5H_2O$ (Riedel-de Haën 31288) were used without further purification or process. All standard solutions were prepared in high purity water (Millipore, 18.2MΩ).

2.2. Applied Methods

Characterization of the synthesized materials, and other liquid/solid phase analyses were performed by the techniques described in the following subsections.

2.2.1. Powder X-ray Diffraction (PXRD)

X-rays are high energy radiations with wavelengths around 1 Å (10^{-10} m). In electromagnetic spectrum, X-rays are placed between gamma-ray region and the ultraviolet region. Since wavelengths of X-rays are nearly in atomic scale, crystalline structures at the atomic level can be determined using this type of radiation. X-ray diffraction method can be used for the fingerprint characterization of crystalline materials and the determination of their structure. Each crystalline solid has its unique characteristic X-ray powder patterns and these patterns can be used as fingerprints for further comparison. Using databases, material can be identified and using X-ray crystallography packing of the atoms in crystalline structure, interatomic distances and angles can be determined.

X-ray diffraction is one of the most important characterization tools used in industry and science since its discovery in 1912. This method can be used to gather

qualitative and quantitative information about the compounds in the sample (Skoog, et al. 1998).

Throughout the study, a Philips X'Pert Pro instrument at the Center of Material Research in Izmir Institute of Technology was used for Powder XRD analysis. The samples were first ground, then introduced for analysis in the special sample holder. Cu K_α radiation at wavelength of 1.54 Å was used as the source.

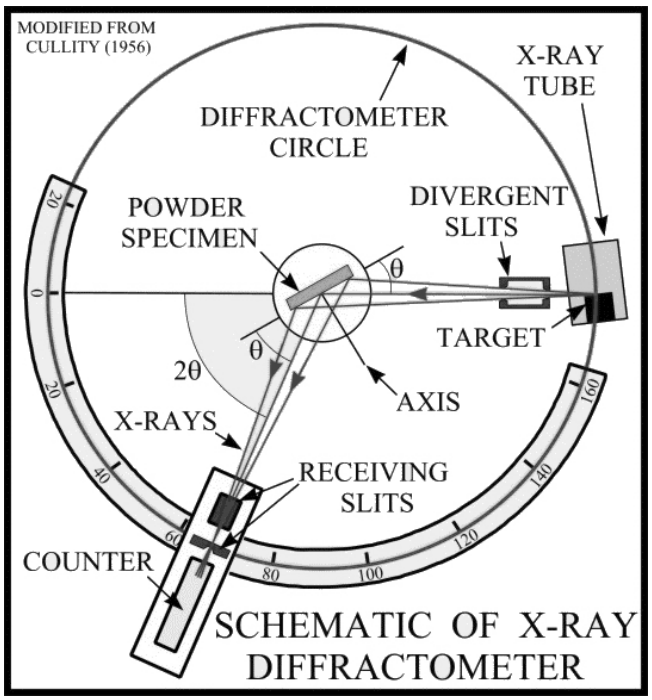

Figure 2.1. Schematic of X-ray Diffractometer
(Source : U.S. Department of the Interior, U.S. Geological Survey 2001)

2.2.2. Scanning Electron Microscopy (SEM)

SEM was invented in the early 1960's and it is now far from being only a specialist laboratory instrument (Lawes and James 1987). The principle of SEM is the scanning of the surface of a solid material in a raster pattern with a beam of electrons as source. The energy of the electron beam can range from a few hundred eV to 100 keV. This beam is focused by one or more condenser lenses into a spot sized 0.4 nm to 5 nm.

By the help of scanning coils or pairs of deflector plates in the electron optical column beam is deflected horizontally and vertically so that scanning occurs in a raster fashion over a rectangular area of the sample surface. The contact of the source electrons with the sample results in the production of backscattered, secondary and Auger electrons as well as X-ray fluorescence photons and various other photons. Basically, backscattered and secondary electron signals are used to study the surfaces (Skoog, et al. 1998, Strobel and Heineman 1989). Backscattered electrons are elastically reflected source electrons and secondary electrons are the emitted electrons from the surface atoms. Those are detected by photomultiplier tube and finally, the 2D or 3D image is displayed on the CRT monitor. Since electrons interact with air molecules both by being scattered and absorbed, a high vacuum media is essential for the quality of analysis.

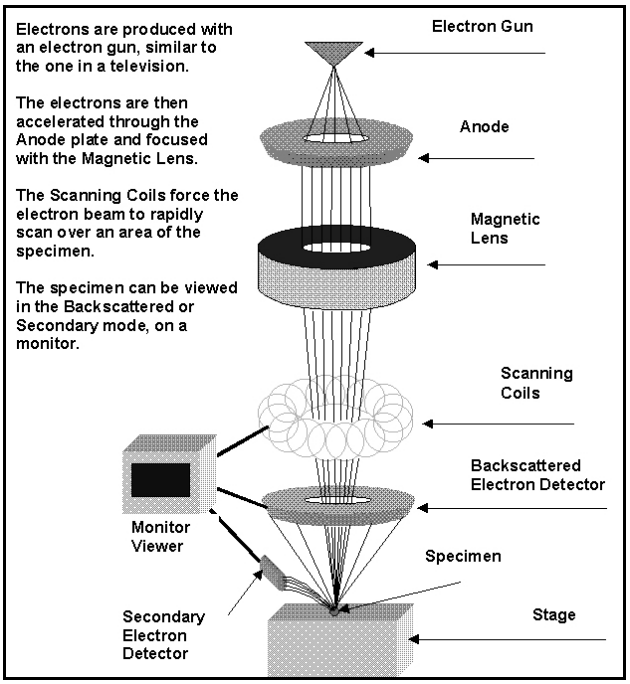

Figure 2.2. Schematic of Scanning Electron Microscopy
(Source: Renssealer Polytechnic Institute 2007)

Throughout the study, SEM/EDS characterizations were performed by a Philips XL-30S FEG model instrument. The powder samples were attached onto adhesive carbon tapes supported on metallic disks. Sample surfaces were then observed at

different magnifications and the images were recorded. Elemental EDS analysis was performed at randomly selected areas on the solid surfaces each being approximately 20μm×20μm in dimension. EDS mapping was carried out at 1000x magnification with a voltage applied at 18 kV under vacuum conditions of $3.5x10^{-5}$ mbar.

2.2.3. Transmission Electron Microscopy (TEM)

In transmission electron microscopy (TEM), a beam of electrons is transmitted through a specimen to form an image. At the top of the microscope, electrons are emitted by the "light source" and travel through vacuum in the column of the microscope. Just like the glass lenses focusing the light in the light microscopes, electromagnetic lenses are used to focus the electrons into a very thin and dense beam. The electron beam then passes through the sample studied. Density of the material present in the sample causes some of the electrons to be scattered and disappeared from the beam. Unscattered electrons hit a fluorescent screen, a layer of photographic or a CCD camera which gives rise to a "shadow image" of the sample with its different parts displayed in varied contrast according to their density (Wikipedia 2007e).

A light microscope presents a magnification that is limited by the wavelength of light while a TEM instrument uses electrons as “source” and the much lower wavelength of electrons makes thousand times better resolution than a light microscope possible. Objects in size of a few Angstroms (10^{-10} m) can be observed by TEM technique. New generation high resolution instruments can be used to study materials in near atomic levels. So TEM is a valuable tool in medical, physical, biological and materials research (Nobel Web AB 2007).

Although TEM is one of the most advanced surface analysis techniques, it is an expensive and destructive technique. There are some restrictions for materials that are sensitive to electron beam radiation, resulting in a loss of crystallinity and mass. Sample preparation is another problem and it is a specialist issue.

The TEM instrument used in this study is a Tecnai F20 from FEI, Netherlands. It was operated at 200 kV acceleration voltage. Sample preparation was performed as follows: Some of the sample powder was dispersed in EtOH using ultrasonic bath. Subsequently, a drop of the dispersion was applied to a holey carbon TEM support grid; excess solution was blotted off by a filter paper.

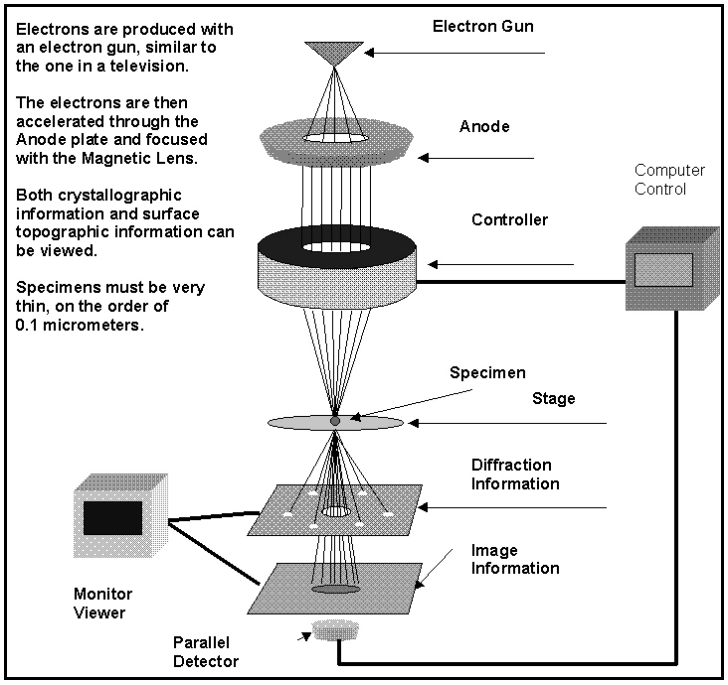

Figure 2.3. Schematic of Transmission Electron Microscopy
(Source: Renssealer Polytechnic Institute)

2.2.4. Electron Energy Loss Spectrometry (EELS)

When electron beam is incident into specimen, part of the electrons is inelastically scattered and undergo partial loses in their energy. Elemental composition and atomic bonding state can be determined by analyzing the energy with the spectroscope attached under the electron microscope (Electron Energy Loss Spectroscopy). Because the analyzing region can be selected from part of the enlarged electron microscopic image, one can analyze very small region. Moreover, by selecting electrons with a specific loss energy by a slit so as to image them, element distribution in specimen can be visualized (Elemental Mapping) (Kyoto University 2007).

EELS analyses in this study were run at a EM 912 from LEO, Germany operated at 120 kV acceleration voltage. Sample preparation is same as for TEM.

2.2.5. X-Ray Photoelectron Spectroscopy (XPS)

X-Ray Photoelectron Spectroscopy (XPS) is also known as Electron Spectroscopy for Chemical Analysis (ESCA). Since its invention by K. Siegbahn, XPS has been a powerful surface technique to determine chemical composition and moreover to provide information about the structure and oxidation state of the compounds in interest. The theory is based on the detection of kinetic energies of emitted core electrons by source X-ray photons. The energy of source photon is fixed and the kinetic energy of the emitted electron can be detected, so binding energy is simply the difference of these two energies. Binding energy of an electron is characteristic of the atom and orbital from which the electron was emitted. Qualitative and quantitative elemental analysis can thus be achieved in a very sensitive manner. Moreover, since binding energy of core electron varies slightly with the oxidation state and charge density of the atom in interest (chemical shifts), it is possible to determine the oxidation state and get information about bonding type. Like TEM, XPS is also an expensive and destructive technique (Skoog, et al. 1998).

2.2.6. Brunauer-Emmett-Teller (BET) Surface Area Analysis

Gas sorption (both adsorption and desorption) at the surface of dry solid powders is the mostly used method for determining the surface area of these powders. In a gas sorption method, firstly the material is heated and degassed to remove previously adsorbed molecules. Then known doses of an inert gas, such as nitrogen, are introduced and the gas is adsorbed (or desorbed). The sample material is placed in a vacuum chamber at a constant and very low temperature, and the pressure upon is varied in a wide range to obtain adsorption and desorption isotherms. Various amounts of gas molecules will be adsorbed or desorbed at different doses of the gas. Since the area occupied by one gas molecule is known, an appropriate adsorption model can be used to determine the total surface area of the sample. The most well known isotherm equation for multilayer adsorption is the equation derived by Brunauer, Emmett, and Teller in 1938. So the surface area analysis technique based on gas

adsorption/desorption and this equation is named as BET Surface Area Analysis (Becman Coulter Inc. 2006).

2.2.7. Zeta - Meter

Each colloidal microscopic particle in a suspension, having a surface charge, produces a difference in electrical potential between its surface and the bulk of the suspension. This difference, in millivolts, is called the zeta potential.

Zeta potential, ξ, can be easily determined because when the suspension is subjected to a direct current (DC) between two ends, charged colloid will move with a velocity proportional to its zeta potential. This phenomenon, movement of charged particles through two ends of a voltage, is called “electrophoresis”.

Determination of zeta potential is important to more fully understand the bulk properties of many suspensions because the key for many bulk-scale processes is again the control of individual colloids.

In this study, zeta-potentials were determined with a Zeta-Meter 3.0+ unit by Zeta-Meter, Inc. with molybdenum anode and platinum cathode.

2.2.8. Flame Atomic Absorption Spectrometry (FAAS)

Atomic Absorption Spectrometry (AAS) is applied to determine trace amounts of elements in various environmental and biological matrices. This technique is sensitive and selective in addition to its simplicity, and wide field of applications, and high sampling rate especially for flame atomixation. Determination of more than six dozen elements is possible by Atomic Absorption technique. In general, the detection limit interval changes from few tenths to part per billion (in electrothermal atomization techniques) or from few tenths to part per million (in ordinary flame atomization) (Jenniss, et al. 1997).

Each element absorbs specific wavelength of light needed to excite electrons from an energy level to other higher energy level. This principle is used in AAS; if an element of interest is present in the sample, a characteristic wavelength of light is absorbed and the absorbance is related to the amount of this element. To produce a light

exactly with the same energy of excitation, hallow-cathode lamps containing tungsten anodes and hollow cathodes made of the element to be determined are used. The sample must be atomized, and emitted electromagnetic radiation is passed through vaporized sample. Since some of the radiation is absorbed by the atoms in the sample, the amount of absorbed radiation increases as the number of atoms increases in the vapor.

AAS instrument consists of three major components; a light source, an atomizaer for the production of gaseous atoms, and a detector for the measurement the specific light absorbed. Diagram of a standard AAS instrument is given in Figure 2.4

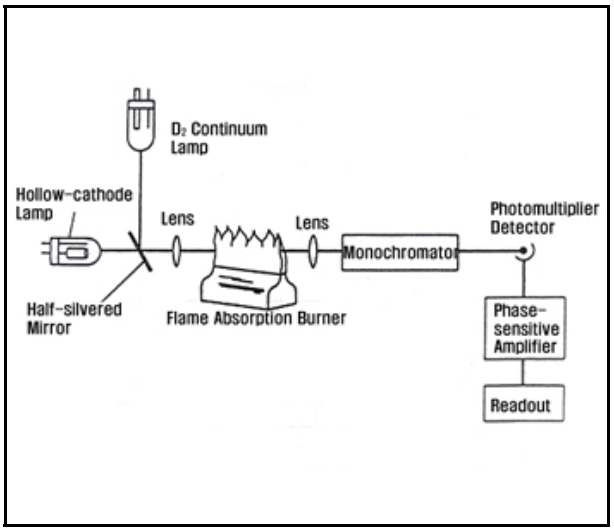

Figure 2.4. Schematic of Flame Atomic Absorption Spectrometer
(Source: Korea Atomic Energy Research Institute 2007)

In this study a Thermo Elemental SOLAAR M6 Series Atomic Absorption Spectrometer with air-acetylene flame was used to determine aqueous cobalt and copper concentrations. Seperate hollow cathode lamps radiating at wavelengths of 240.7 (Co) and 224.8 (Cu) were used in the instrument for the determination of Co and Cu amounts.

2.3. Synthesis

Synthesis of the materials throughout this study are discussed in the subsections below.

2.3.1. Nanoscaled Zero-Valent Iron (nZVI)

Synthesis of nZVI is based on borohydride reduction of Fe(II) (Wang and Zhang 1997, Wang, et al. 2006a). In this study, iron(II) chloride tetrahydrate ($FeCl_2$. $4H_2O$) and sodium borohydride ($NaBH_4$) were used for iron(II) and borohydride sources respectively. The proposed reaction is:

$$Fe^{2+} + 2BH^- + 6H_2O \rightarrow Fe^0 + 2B(OH)_3 + 7H_2 \uparrow$$

For the synthesis of 1.5 g of nZVI; 5.34 g $FeCl_2.4H_2O$ was dissolved in a 4/1 (v/v) ethanol/water mixture (24 ml ethanol + 6 ml deionized water) and stirred on a magnetic stirrer.

On the other hand, 1 M sodium borohydride solution was prepared; 3.05 g $NaBH_4$ was dissolved in 100 ml of deionized water. The final BH_4^- / Fe^{2+} ratio is adjusted to 3, since excess borohydride is needed for better growth of nanoparticles.

The borohydride solution is poured in a burette and added dropwise to the iron(II) solution, while still stirring on magnetic stirrer. Black solid particles immediately appeared after the first drop of sodium borohydride solution. After adding the whole borohydride solution, the mixture was left for another 10 minutes of stirring.

To separate the black iron nanoparticles from the liquid phase, vacuum filtration technique was used. Two sheets of blue band Whatman filter papers were used in filtration. At this point, solid particles were washed at least three times with 25 ml portions of absolute ethanol to remove all of the water. This washing process is probably the key step of synthesis since it prevents the rapid oxidation of zero-valent iron nanoparticles. Synthesized nanoparticles were finally dried in oven at 50 ^oC overnight. Drying in evacuated ovens must be avoided because this would cause Fe nanoparticles to spontaneously ignite upon exposure to air.

2.3.2. Kaolinite Supported nZVI (kaol-nZVI)

Synthesis of kaol-nZVI is based on borohydride reduction of Fe(II) (Wang and Zhang 1997, Wang, et al. 2006a). For the synthesis, iron(II) chloride tetrahydrate ($FeCl_2$. $4H_2O$) and sodium borohydride ($NaBH_4$) were used for iron(II) and borohydride sources respectively. Kaolinite-supported nZVI was synthesized such that final (kaolinite): (zero-valent iron) ratio was 1:1, 2:1 or 5:1 (m/m). For 1:1 ratio sample; 5.34 g $FeCl_2.4H_2O$ was dissolved in a 4/1 (v/v) ethanol/water mixture (24 ml ethanol + 6 ml deionized water). Then 1.5 g kaolinite was added to this solution and the mixture was held on a magnetic stirrer to be mixed.

On the other hand, 1 M sodium borohydride solution was prepared; 3.05 g $NaBH_4$ was dissolved in 100 ml of deionized water such that total BH_4^- / Fe^{2+} ratio is 3, keeping in mind that excess borohydride is needed for a successful synthesis.

Borohydride solution is then added dropwise to the iron(II) - kaolinite - water mixture described above, while still stirring on a magnetic stirrer. Black solid particles immediately appeared after adding the first drop of sodium borohydride solution. After the addition of the borohydride solution was completed, the mixture was left for excess 10 minutes of stirring.

To separate the black iron nanoparticles from the liquid phase, vacuum filtration was used. Two sheets of blue band Whatman filter papers were used in filtration. At this stage, solid particles were washed at least three times with 25 ml portions of absolute ethanol to remove all of the water. Last step of the synthesis is to dry the synthesized nanoparticles in oven at 50 ^oC overnight.

2:1 and 5:1 kaol:nZVI were synthesized following the same path except the amounts of chemicals are different. Table 2.1 gives the amounts of chemicals used in each of the synthesis trials.

Table 2.1. Amounts of chemicals used in the synthesis of kaol-nZVI materials**.**

Kaol:nZVI	**1:1**	**2:1**	**5:1**
Kaolinite (g)	1.50	1.50	1.50
$FeCl_2$. $4H_2O$ (g)	5.34	2.67	1.068
ethanol / water (ml/ml)	24/6	16/4	16/4
$NaBH_4$ (g) / water (ml)	3.05 / 100	1.52 / 50	0.61 / 25

2.3.3. Montmorillonite Supported nZVI (Mont-nZVI)

Synthesis of montmorillonite-supported nanoscaled zero-valent iron, mont-nZVI, is achieved via the same method given above for the synthesis of kaol-nZVI except that montmorillonite is used instead of kaolinite. Table 2.1 is also valid for mont-nZVI in case kaolinite is replaced with montmorillonite.

2.4. Sorption Experiments

Throughout this study, Co^{2+} solutions were prepared as follows: 1.010 g of $CoCl_2.6H_2O$ was dissolved in 250 mL of high purity water in a volumetric flask to yield 1000 mg/L Co^{2+} stock solution that was then used in preparing solutions with lower concentrations by serial dilution.

For the preparation of Cu^{2+} solutions, 0.915 g of $Cu(NO_3)_2.2.5H_2O$ was dissolved in 250 mL of high purity water and the resulting 1000 mg/L stock solution of Cu^{2+} was used to prepare solutions with lower concentrations by serial dilution. All experiments were run for Co^{2+} and Cu^{2+} separately and no other competing ions were added.

Unless stated otherwise, all adsorption experiments were carried out at ambient temperature and pressure using 50 mL falcon tubes. The mixtures in tubes were kept on an orbital shaker operating at 350 rpm. After 24 hours of shaking (except for the kinetic experiments), the tubes were centrifuged at 6000 rpm. The supernatant solutions were transferred into clean falcon tubes and acidified to 1% v/v with concentrated nitric acid. The solutions were then kept in fridge until use, and were diluted in proper ratios before analysis by AAS.

2.4.1. Effect of Volume/Mass (V/m) Ratio

0.05 g of 5:1 kaol-nZVI was added into 10, 20, 30 and 40 mL of 50 mg/L or 500 mg/L metal solutions (of Co^{2+} or Cu^{2+}) in 50 mL falcon tubes. The resulting V/m ratios are 200, 400, 600 and 800 (mL/g), respectively. The tubes were shaken on an orbital shaker at 350 rpm for 24 hours. After centrifugation, the supernatant solutions were

transferred into clean falcon tubes and concentrated nitric acid was added to these solutions to have a final HNO_3 concentration of 1% (v/v). The solutions were kept in fridge until AAS analysis. Similar experiments were performed for 5:1 mont-nZVI.

2.4.2. Kinetics

To determine the effect of contact time of metal solutions with sorbents, 0.05 g of kaol-nZVI sample was added into 40 mL portions of 100 mg/L metal solutions (Co^{2+} or Cu^{2+}). The tubes were removed from the shaker after 1 min, 5 min, 10 min, 30 min, 1 h, 2h, 4h, 8h, 16h and 24 h of contact time. After centrifugation and acidification, supernatant solutions were kept in fridge until analysis. Experiments were run for 1:1, 2:1 and 5:1 kaol-nZVI separately. Similar experiments were also performed for 1:1, 2:1 and 5:1 mont-nZVI samples.

2.4.3. Effect of Initial Metal Concentration

The effect of initial metal concentration on the extent of uptake were investigated as follows: 0.05 g of kaol-nZVI sample was added into 40 mL portions of metal solutions (Co^{2+} or Cu^{2+}) having concentrations of 1 mg/L, 5 mg/L, 10 mg/L, 50 mg/L, 100 mg/L, 250 mg/L and 500 mg/L. The mixtures were shaken on the orbital shaker for 24 hours and then removed for centrifugation. The supernatant solutions were then acidified and kept in fridge until analysis. The experiments were done using 1:1, 2:1 and 5:1 kaol-nZVI, separately. Similar experiments were also performed using 1:1, 2:1 and 5:1 mont-nZVI samples. For the sake of comparison, parallel experiments were performed using pure nZVI, pure kaolinite, and pure montmorillonite.

2.4.4. Effect of pH

The pHs of 40 mL portions of metal solutions (Co^{2+} or Cu^{2+}) were adjusted to 4, 6, 8 and 10 using 0.1 M or 3 M HNO_3 or NaOH. Then 0.05 g of 5:1 kaol-nZVI was added into these solutions in falcon tubes and the mixtures were shaken for 24 hours.

After separation of liquid and solid phases by centrifugation, the solutions were acidified and kept in the fridge until analysis. The pH of the solutions were measured at the beginning and the end of shaking process. Similar experiments were performed also for 5:1 mont-nZVI.

2.4.5. Repetitive Applications

To study the reusability of synthesized materials, a series of repetitive experiments were performed. In each experiment, 0.2 g of 5:1 kaol-nZVI sample were added into 10 ml of 5 mg/L or 100 mg/L metal solution (Co^{2+} or Cu^{2+}) in a 50 mL falcon tube. After a shaking period of 45 minutes, the mixture was centrifuged, the supernatant solution were transferred into a clean tube and acidified. Then, a 10 mL portion of the fresh metal solution possessing the same concentration as the previous portion was added onto the solid sample that remained in the tube. After a further shaking for 45 minutes, the liquid phase was separated again and kept for the analysis. These trials were repeated such that 5:1 kaol-nZVI was repeatedly exposed to eight doses of 10 mL solution portions. Similar experiments were performed also for 5:1 mont-nZVI.

CHAPTER 3

RESULTS AND DISCUSSION

3.1. Characterization of Synthesized Materials

Discussions upon characterizations of nZVI, kaol-nZVI and mont-nZVI are provided in the following subsections.

3.1.1. Nanoscaled Zero-Valent Iron (nZVI)

Powder XRD patterns of nZVI samples aged for various periods of time under ambient conditions are presented in Figure 3.1. The characteristic diffraction line at 44.7^{o} 2 theta degrees indicates that zero-valent iron is predominantly present in all samples.

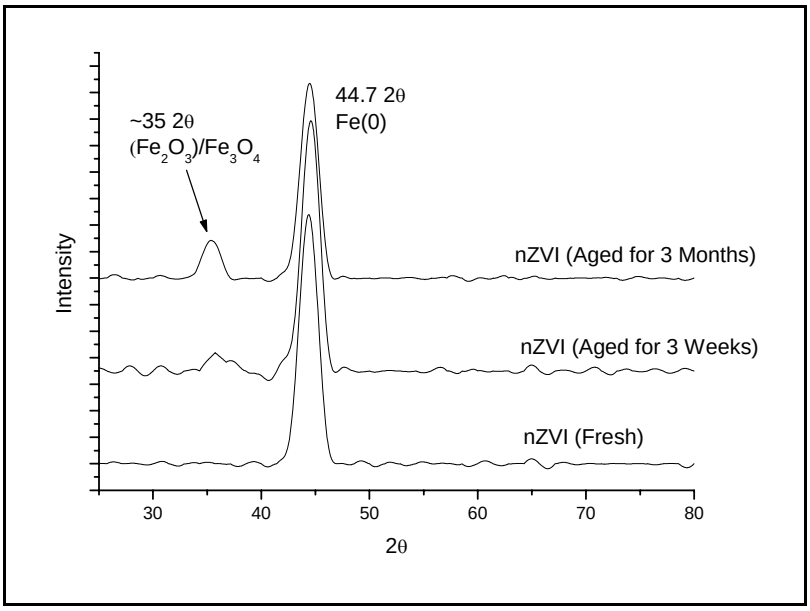

Figure 3.1. Comparative Powder XRD patterns of nZVI samples aged for various times

In the XRD pattern of freshly synthesized nZVI, no signal for the iron oxides (hematite, Fe_2O_3 or magnetite, Fe_3O_4) was observed. However this can not be solely used as an evidence for the complete absence of iron oxide in the sample as XRD patterns reflects the crystallinity of a certain material rather than its oxidation state. This topic is elaborated further in light of the HR-TEM images provided in this section. The XRD pattern of a sample aged for 3 weeks and another aged for 3 months are demonstrated also in Figure 3.1. Weak signals of iron oxides appeared at 2θ of 36^o for nZVI samples aged for 3 weeks but these signals became clearer for the samples aged for 3 months. This is in line with previous results stating that iron on a nano-scale can resist oxidation under atmospheric conditions for a long period (Liu, et al. 2005a, Liu, et al. 2005b).

Although they are called "zero-valent iron nanoparticles", it should be noted that the spherical iron particles form chain-like structures the length of which might be larger than a micron rather than existing in separate nanoparticles. SEM images of freshly synthesized iron nanoparticles at 20000x and 100000x magnification are presented in Figure 3.2. The images resemble the previously reported ones (Li and Zhang 2006, Sohn, et al. 2006, Li, et al. 2006). It can be observed that iron nanospheres, having diameters of 50-100 nm exist in contact with each other and form chains having diameters of again 50-100 nm. This nearly linear orientation is due to the magnetic properties of iron species (Feng and Lim 2007, Ngo and Pileni 2001, Korth, et al. 2006).

High Resolution Transmission Electron Microscopy (HR-TEM) provides opportunity for more detailed study of iron nanoparticles. In Figure 3.3 (a), chainlike structure of iron nanoparticles is clearly observed in agreement with SEM results. The spheres having diameters of 40-60 nm can be distinguished from each other. With closer inspection, the color contrast that corresponds to metallic iron and iron oxide phases can be distinguished in TEM images. Dark regions are concentrated in the centers of nanospheres while the lighter regions are mainly on the surfaces. As discussed in section 2.2.3, a TEM instrument is designed so that elements with higher atomic numbers seem darker than the ones with lower atomic numbers. This information leads to the conclusion that average atomic number of central elements is higher than the average atomic number of surface elements. This phenomenon is systematically explained by core-shell structure discussed in section 1.3. According to this model, the core of iron nanospheres is formed of metallic iron and the surface (shell) is formed of iron oxides. Our TEM images are in line with the core-shell model

and the images resemble the previously reported ones (Li and Zhang 2007, Li, et al. 2006, Zhang and Elliot 2006).

As a further evidence, elemental mappings for iron and oxygen performed by Electron Energy Loss Spectrometry confirms the earlier conclusion that inner regions (core) consist of elemental iron only, while the surfaces (shell) contain both iron and oxygen species as shown in Figure 3.4.

The type of crystalline iron phase was analyzed using Selected Area Electron Diffraction (SAED). A typical SAED image for an iron nanoparticle is presented in Figure 3.5. (a). In addition, the diffraction image was transformed into a "powder x-ray" diffraction graph, Figure 3.5. (b), to facilitate its comparison with the data-base. According to the results zero-valent iron has the space group Im-3m indicating that it is α-Fe (ferromagnetic, BCC lattice structure).

BET and Langmuir surface area values were determined as 14.19 m^2/g and 51.41 m^2/g, respectively, for nZVI. Some of the BET surface area values reported in literature are 14.5 m^2/g (Sun, et al. 2006), 33.5 m^2/g (Wang and Zhang 1997) and 36.5 m^2/g (Lie, et al. 2005b). In comparison, commercially available Fe powder (<10 μ) has a specific surface area of just 0.9 m^2/g (Wang and Zhang 1997). The increase in specific surface area means an increase in the total amount of iron on the surfaces. Since the active site for the remediation is the iron surface itself, samples with a high surface area have greater remediation capacity.

To determine the isoelectric point of iron nanoparticles, their zeta potential at various pH media were determined by a Zeta-Meter 3.0+ instrument. The results are provided in Figure 3.6. The isoelectric point (IEP), where the surface charge of iron nanoparticles is zero, arises nearly at pH 8.1 which is in agreement with the previously reported values (Li, et al. 2006, Zhang and Elliot 2006, Li and Zhang 2006, Sun, et al. 2006). This is relatively a high IEP and means that within natural pH range, nZVI particles have positive surface charges. It is notable that despite their positive surface charges, zero-valent iron nanoparticles have great capacity for the stabilization of positively charged metal ions, the thing elaborated further within the context of the discussion of the interaction mechanism.

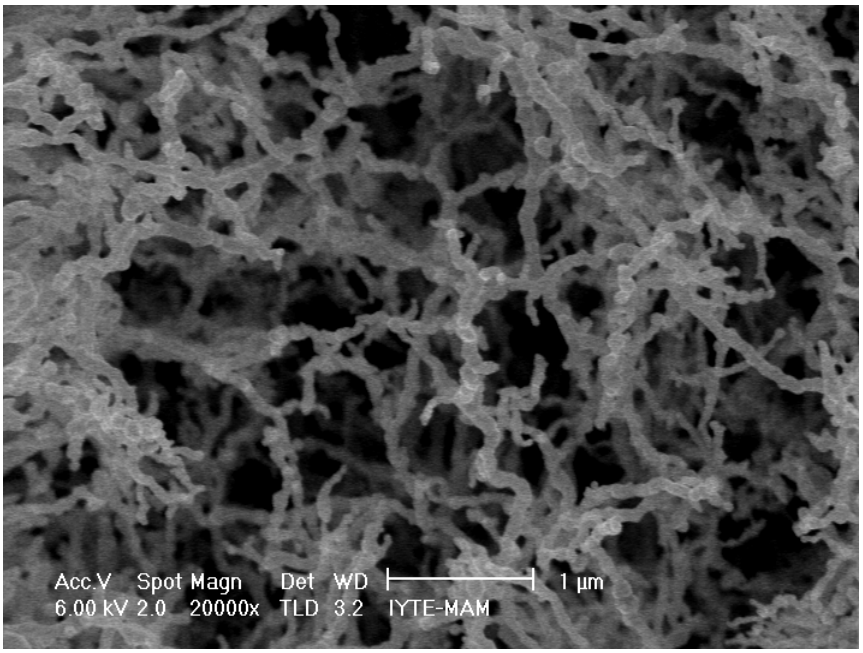

(a)

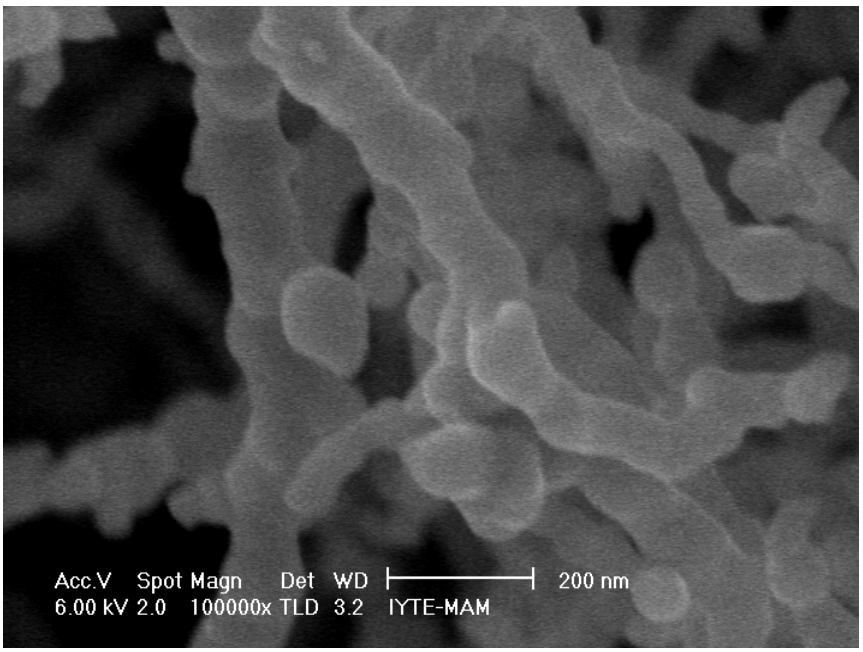

(b)

Figure 3.2. Characteristic SEM images of nZVI at (a) 20000x and (b) 100000x magnification

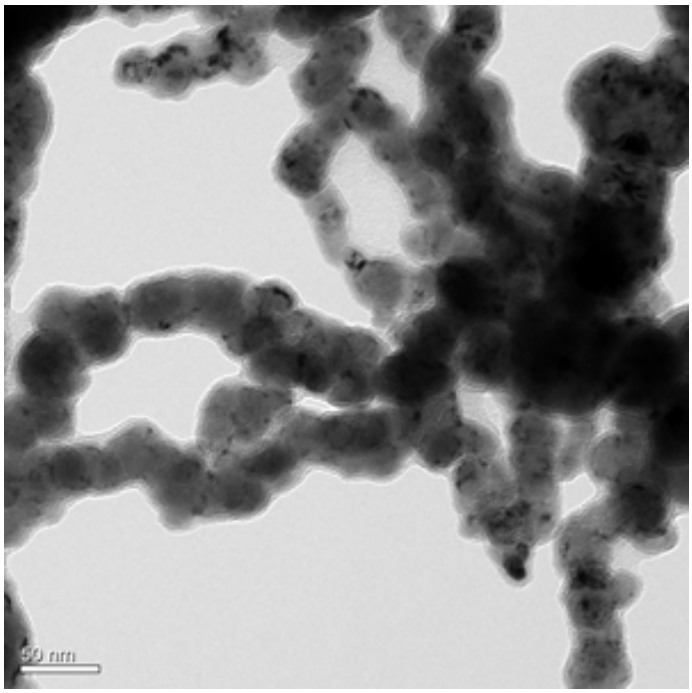

(a)

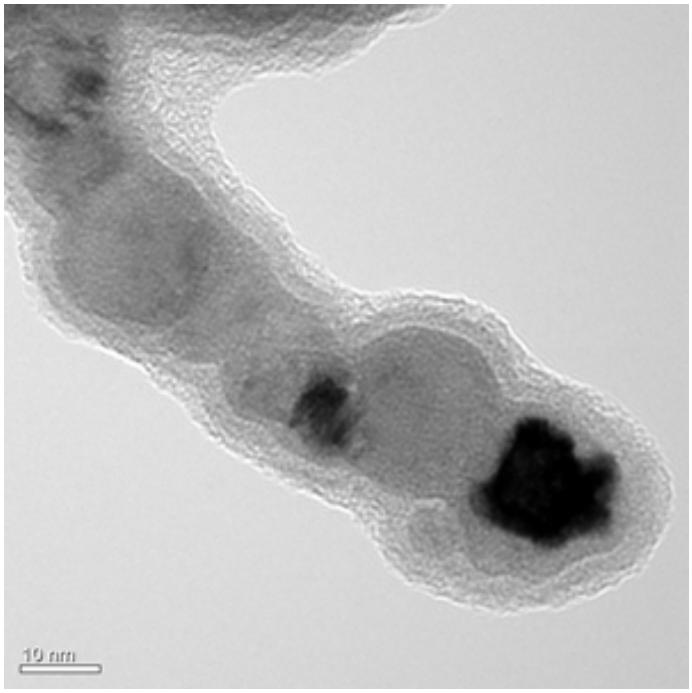

(b)

Figure 3.3. High Resolution Transmission Electron Microscope Images of nZVI

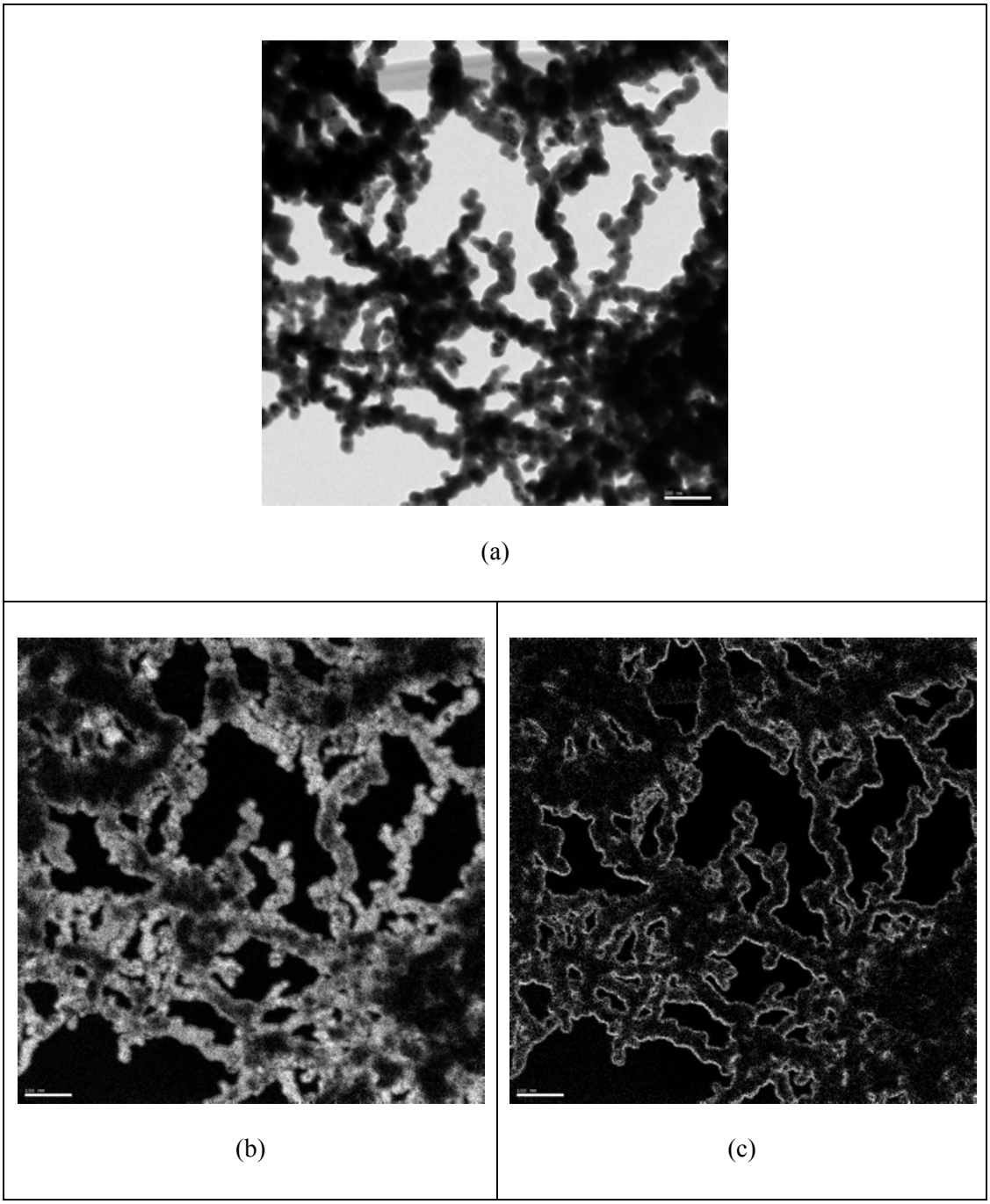

(a)

(b)

(c)

Figure 3.4. (a) Overall EELS image, (b) EELS iron mapping, (c) EELS oxygen mapping of zero-valent iron nanoparticles

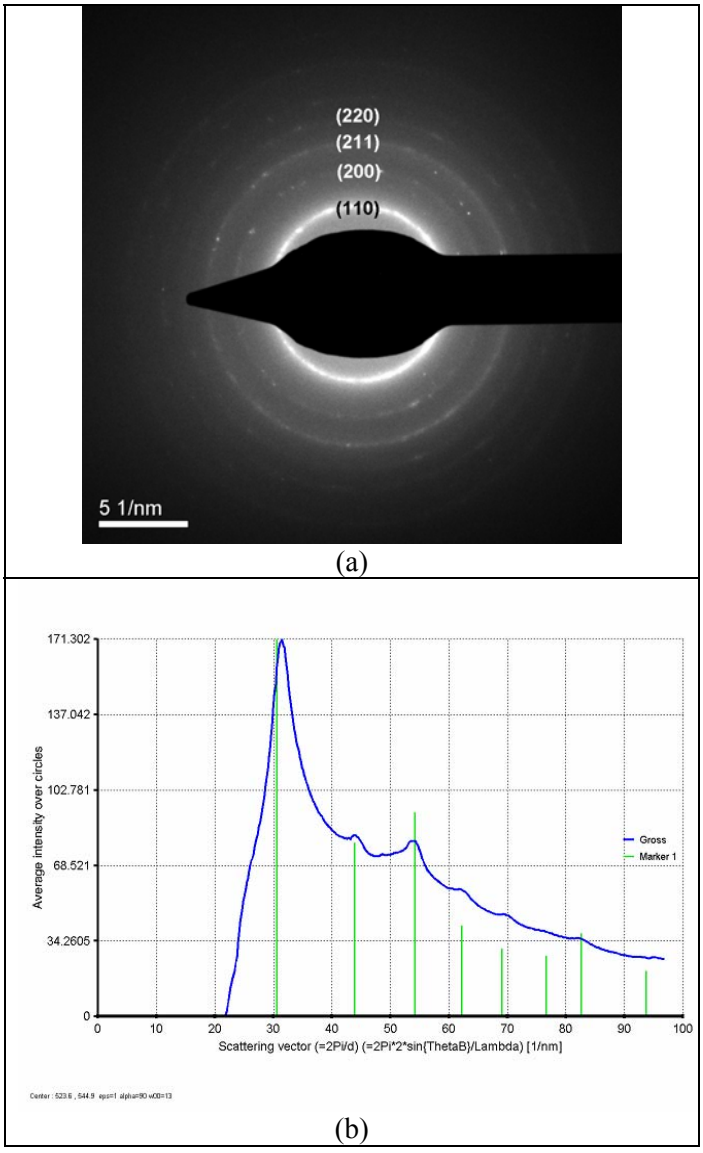

Figure 3.5. Selected Area Electron Diffraction (SAED) of nZVI (a) the original image (b) converted to PXRD pattern.

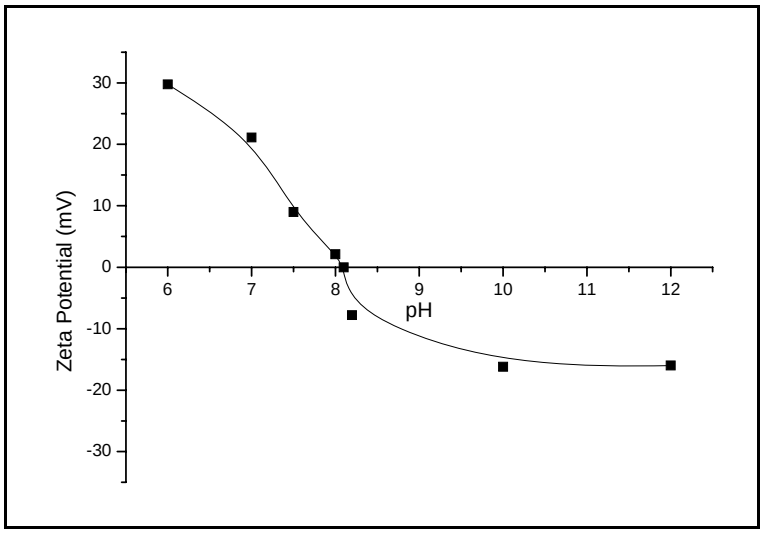

Figure 3.6. Zeta Potentials of nZVI at various pH

3.1.2. Kaolinite-Supported Nanoscaled Zero-Valent Iron (kaol-nZVI)

Modified iron nanoparticles, such as catalyzed and supported nanoparticles have been synthesized to further enhance the speed and efficiency of remediation. When the reduction of aqueous iron salt is done in the presence of a support material, the agglomeration of iron particles could be prevented, thus offering a higher specific surface area of iron to the aqueous stream. In addition, this material is expected to provide flexibility in the application of iron nanoparticles technology for environmental remediation. No report is yet available in literature on the application of clay minerals for this purpose. Kaolinite is one of the clay minerals that are well-known for their stability within geochemical conditions, ability to act as adsorbents, in addition to their wide availability across the geomedia. Different mass ratios of kaolinite to iron were tested and the reactivity of the produced composites was investigated.

The synthesized kaolinite-supported zero-valent iron nanoparticles appeared in powder form with an opaque black color that resembles largely that of pure nZVI. The samples appeared coarser and possessed a more grayish appearence as the mass ratio of clay increased in the structures. The characterization of synthesized 1:1, 2:1 and 5:1 kaol-nZVI solids were performed by Powder XRD, SEM/EDX, XPS, TEM, Zeta-Meter and BET methods.

The XRD diffraction patterns indicate the presence of iron in its zero-valent oxidation state on kaolinite. Figure 3.7 shows typical XRD diffraction patterns of kaol-nZVI material. The diffraction line near 44.7^{o} 2θ belongs to metallic iron, just as in the case of pure nZVI. Various lines arising from the crystal structure of kaolinite (basically 001 and 002 lines) are also observed.

SEM images of 1:1, 2:1 and 5:1 kaol-nZVI are presented in Figure 3.8. Figures (a) and (b) belong to 1:1 kaol-nZVI. Chainlike aggregates of iron nanoparticles still exist but unlike pure nZVI, separated iron nanospheres having diameters of 40-80 nm can also be observed. These images show that separation of spherical iron nanoparticles is possible in the absence of an organic dispersing agent (like a surfactant). Similar results were reported by using graphite as the supporting material (Zhang, et al. 2006). Images (c) and (d) belong to 2:1 kaol-nZVI and images (e) and (f) belong to 5:1 kaol-nZVI in Figure 3.8. Distinct iron nanospheres can also be distinguished in these structures. The nanoparticles of zero-valent iron are present on the surfaces of kaolinite layers, on the broken ends, and in between the layers of kaolinite structure. The observation that more nanoparticles are present on the edge sites of the clay might be indicative that the active hydroxyl sites of kaolinite layers play a role in the synthesis of zero-valent iron.

The distinct iron nanospheres can be observed more clearly in the TEM images of kaol-nZVI (Figure 3.9). The contrast difference between the center and outer sides of the spheres is indicative of the core-shell structure. Figure 3.9 (a) and (b) correspond to typical TEM images of 1:1 kaol-nZVI, (c) and (d) correspond to 2:1 kaol-nZVI. Images (e) and (f) in the same figure belong to 5:1 kaol-nZVI. For all kaol-nZVI samples, a certain extent of dispersion of nanoparticles is clearly achieved. However, this dispersion does not look uniform, and the sizes of nanospheres show a wide variation within a diameter range predominantly within 10-50 nm. The decrease in particle size, in comparison to unsupported nZVI, leads to allowing a larger fraction of iron nanoparticles to be active for metal uptake.

BET and Langmuir surface area values are given in Table 3.1 for 1:1, 2:1 and 5:1 mont-nZVI species. It is clear that there is a change in specific surface area values with varied kaolinite:nZVI ratio and more effort is still needed to clarify the relation of kaolinite:nZVI ratio and specific surface area.

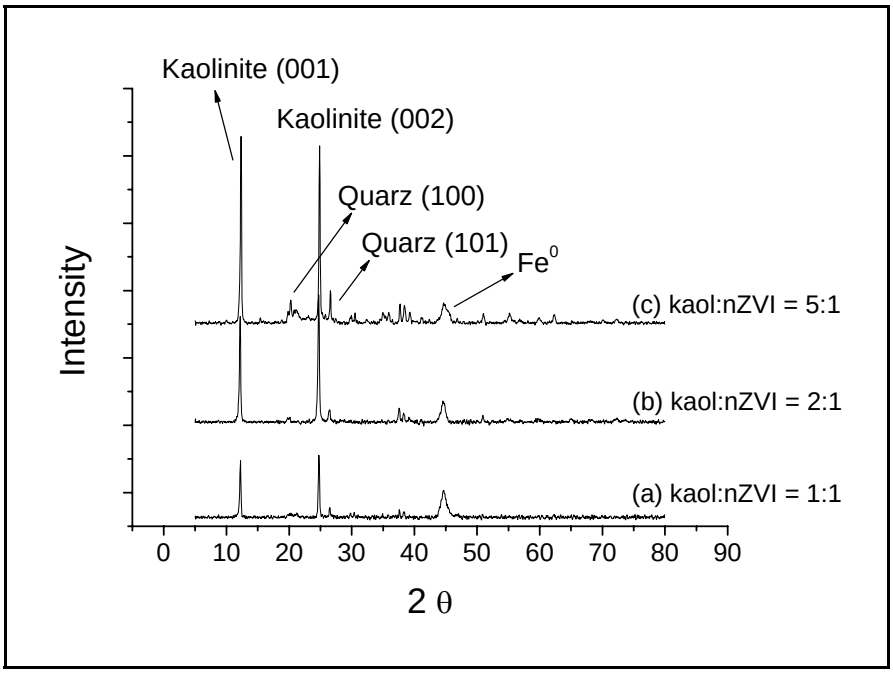

Figure 3.7. XRD patterns of (a) 1:1, (b) 2:1, (c) 5:1 kaol-nZVI

Table 3.1. BET and Langmuir Surface Area Values of kaol-nZVI samples

Surface Area Values (m^2/g)	**Kaolinite:nZVI**		
	1:1	**2:1**	**5:1**
BET	9.55	6.13	6.91
Langmuir	34.80	21.61	24.70

For further characterization, iso-electric points (IEPs) of 1:1, 2:1 and 5:1 kaol-nZVI samples were determined by measuring the zeta potentials at various pH. The trends are given in Figure 3.10 and the IEPs were determined as pH ~6.7, ~7 and ~7 for 1:1, 2:1 and 5:1 kaol-nZVI, respectively. Isoelectric point of pure kaolinite is reported in a wide range and considered around pH 3 (Bragg, et al. 1994).

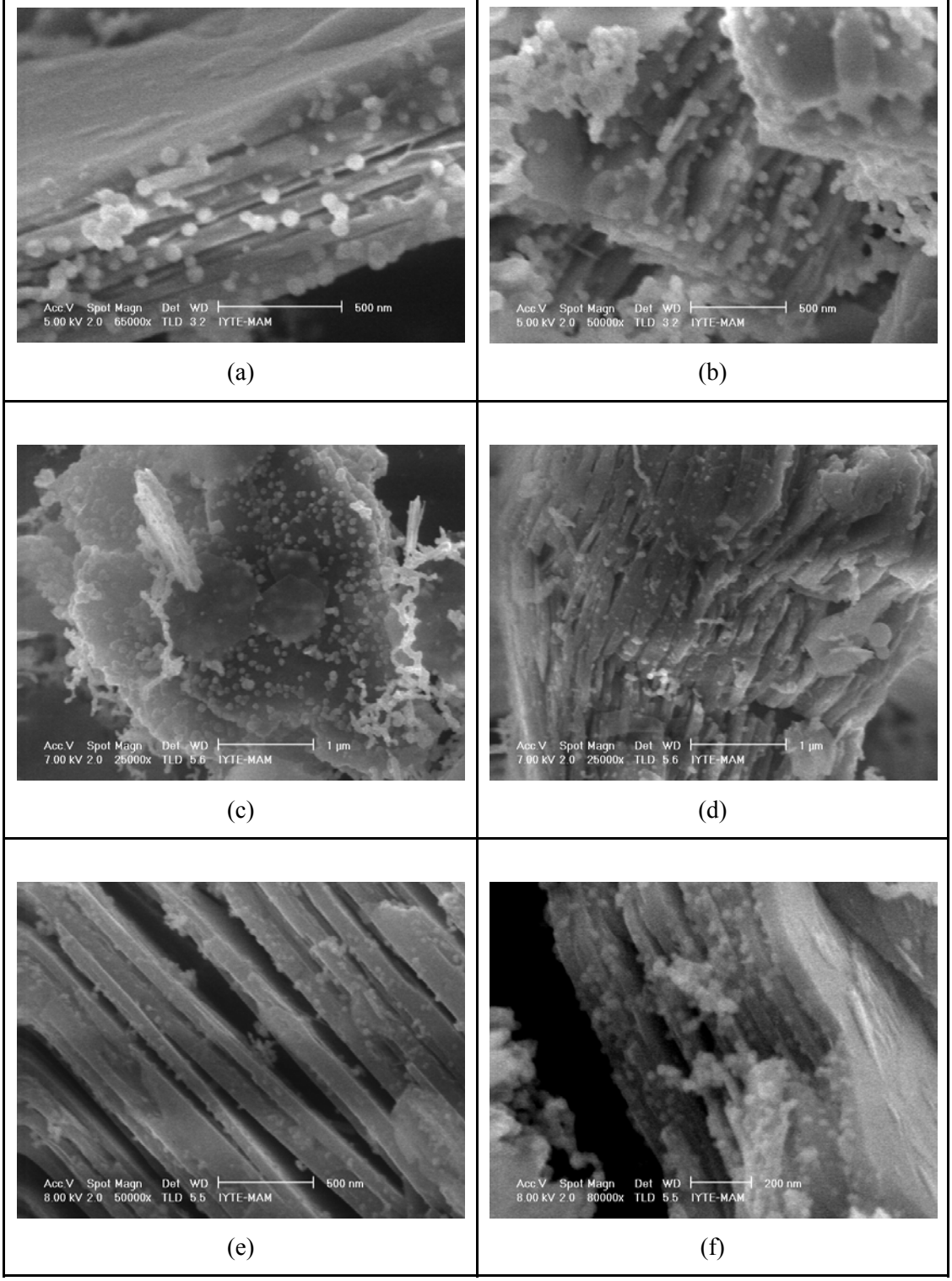

Figure 3.8. SEM images of kaol-nZVI samples. (a) and (b) belong to 1:1, (c) and (d) 2:1, (e) and (f) 5:1 kaol-nZVI.

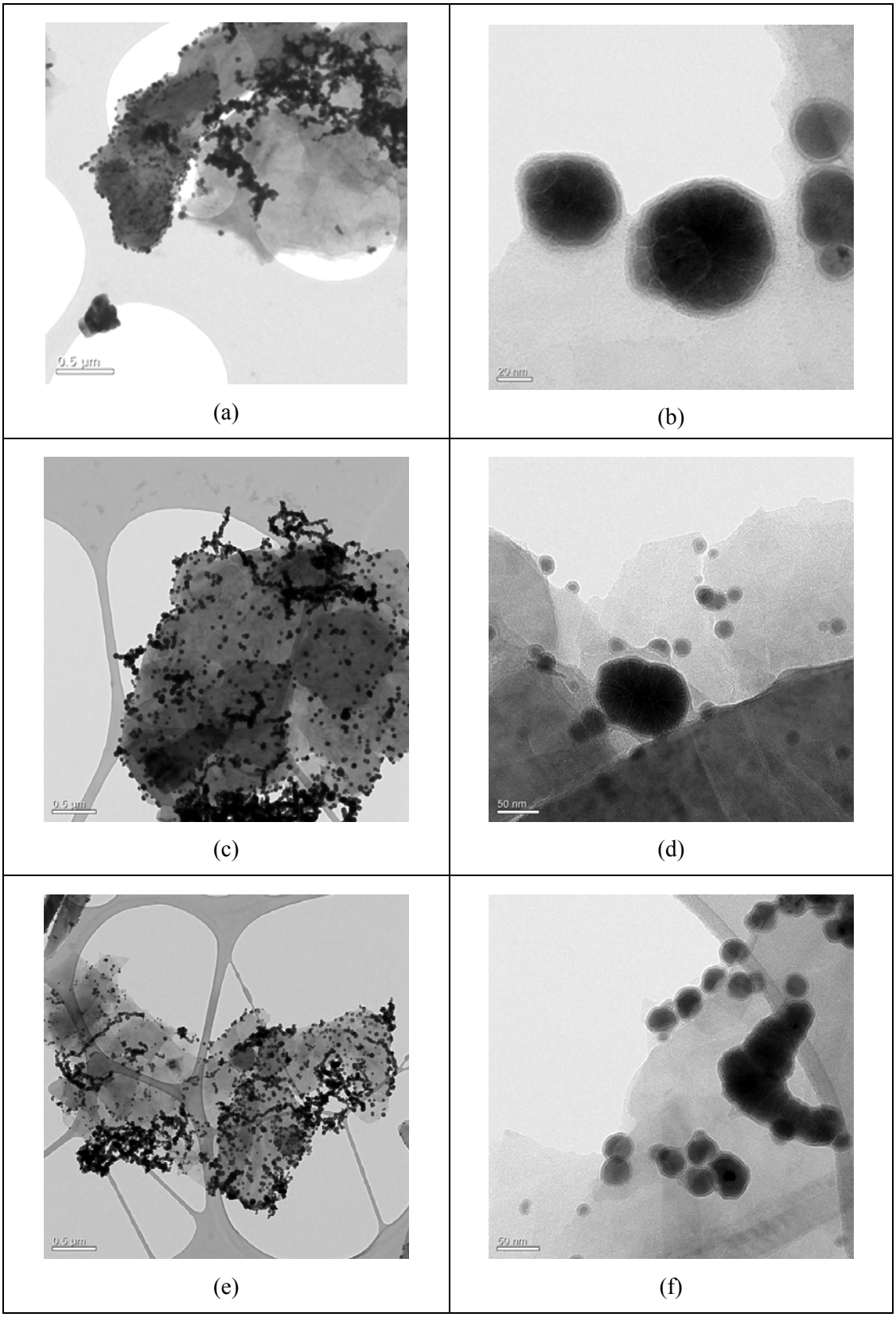

Figure 3.9. TEM images of kaol-nZVI samples. (a) and (b) belong to 1:1, (c) and (d) 2:1, (e) and (f) 5:1 kaol-nZVI.

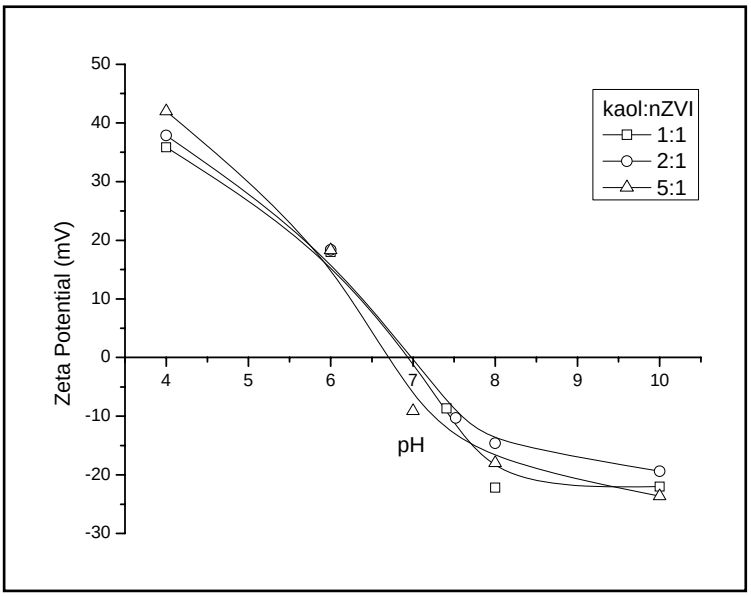

Figure 3.10. Zeta Potentials of 1:1, 2:1 and 5:1 kaol-nZVI at various pHs

3.1.3. Montmorillonite-Supported Nanoscale Zero-Valent Iron (mont-nZVI)

Montmorillonite is among the most widely known clay minerals, and is extensively tried by various researchers across the world in adsorption applications because of its large surface area and relatively wide interlayer space being expandable in aqueous media.

In this study, montmorillonite:nZVI ratio were adjusted as 1:1, 2:1 and 5:1 (m/m). Just like unsupported and kaolinite-supported zero-valent iron nanoparticles, montmorillonite-supported zero-valent iron nanoparticles (mont-nZVI) had a dominant opaque-black appearance. Powder XRD, SEM/EDX, TEM, Zeta-Meter and BET methods were used for the characterization of the synthesized material.

The XRD patterns of 1:1, 2:1 and 5:1 mont-nZVI are given in Figure 3.11. The diffraction line at 2θ of 44.7^{o}, indicates the presence of metallic iron in all three composites. The other diffraction lines are arise from montmorillonite and other associated minerals like illite and quartz, and these lines get more intense as the montmorillonite mass ratio increases in mont-nZVI samples.

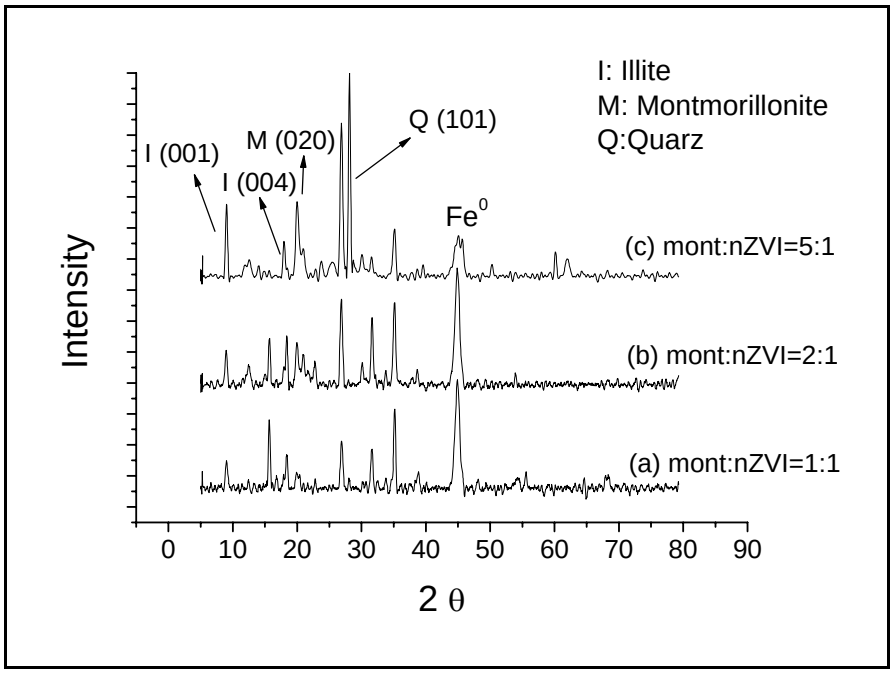

Figure 3.11. XRD Patterns of (a) 1:1, (b) 2:1, (c) 5:1 mont:nZVI

Figure 3.13 presents the SEM images of (a) 1:1, (b) 2:1 and (c) 5:1 mont-nZVI. In all three samples, dispersed zero-valent iron nanoparticles are formed on the surface of montmorillonite. However, the variation of size of nanospheres with the change in montmorillonite:nZVI ratio is unclear and more work is needed in this regard.

Typical TEM images are shown in Figure 3.14 for; (a) 1:1, (b) 2:1 and (c) 5:1 mont-nZVI. Dispersed iron nanospheres on the surface of montmorillonite appear clearly in all three mont-nZVI samples demonstrating the typical core-shell structure with a particle diameter varying within 10-50 nm.

BET and Langmuir surface area values are given in Table 3.2 for 1:1, 2:1 and 5:1 mont-nZVI species. The specific surface area increases as the montmorillonite ratio increases in samples. It is still unclear to what extent does the dispersion of iron nanoparticles enhance the surface area of the material. The optimization of clay:nZVI in a manner that leads to maximizing the dispersion of iron nanoparticles remains a serious goal that requires extensive effort in future work.

The variations of zeta-potential of mont-nZVI species with medium pH are given in Figure 3.12. Isoelectric points arise within pH 3-4 for 1:1, 2:1 and 5:1 mont-nZVI. These points are close to that of pure montmorillonite, ~2.5 (Jaruwong, et al.

2005). In aqueous media, having a pH higher than the given isoelectric point, colloidal particles have a negative surface charge. So within natural pH conditions, mont-nZVI species are expected to have negative surface charges and consequently be more effective in attracting cationic species in comparison to pure nZVI for which the IEP was given earlier to be around 8.1.

Table 3.2. BET and Langmuir Surface Area Values of mont-nZVI samples

Surface Area Values (m^2/g)	**Montmorillonite:nZVI**		
	1:1	**2:1**	**5:1**
BET	34.82	50.00	66.51
Langmuir	185.00	213.56	361.17

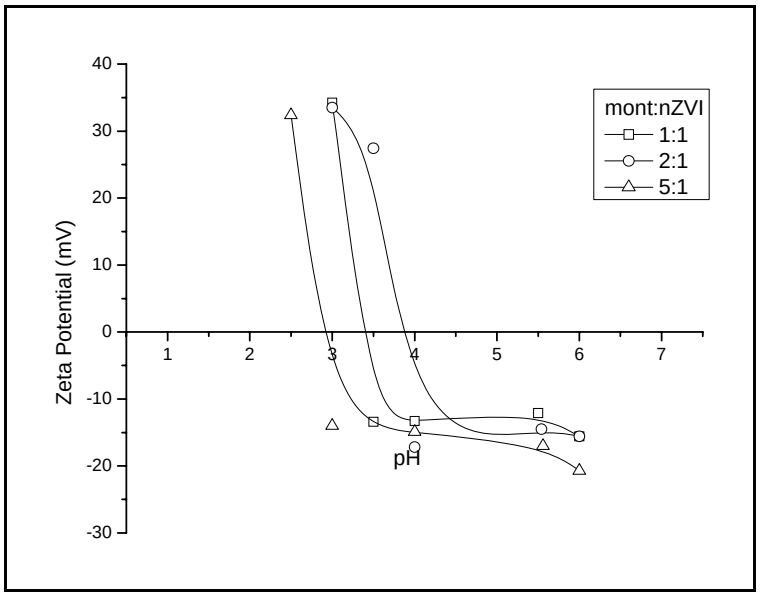

Figure 3.12. Zeta Potentials of mont-nZVI samples at various pHs

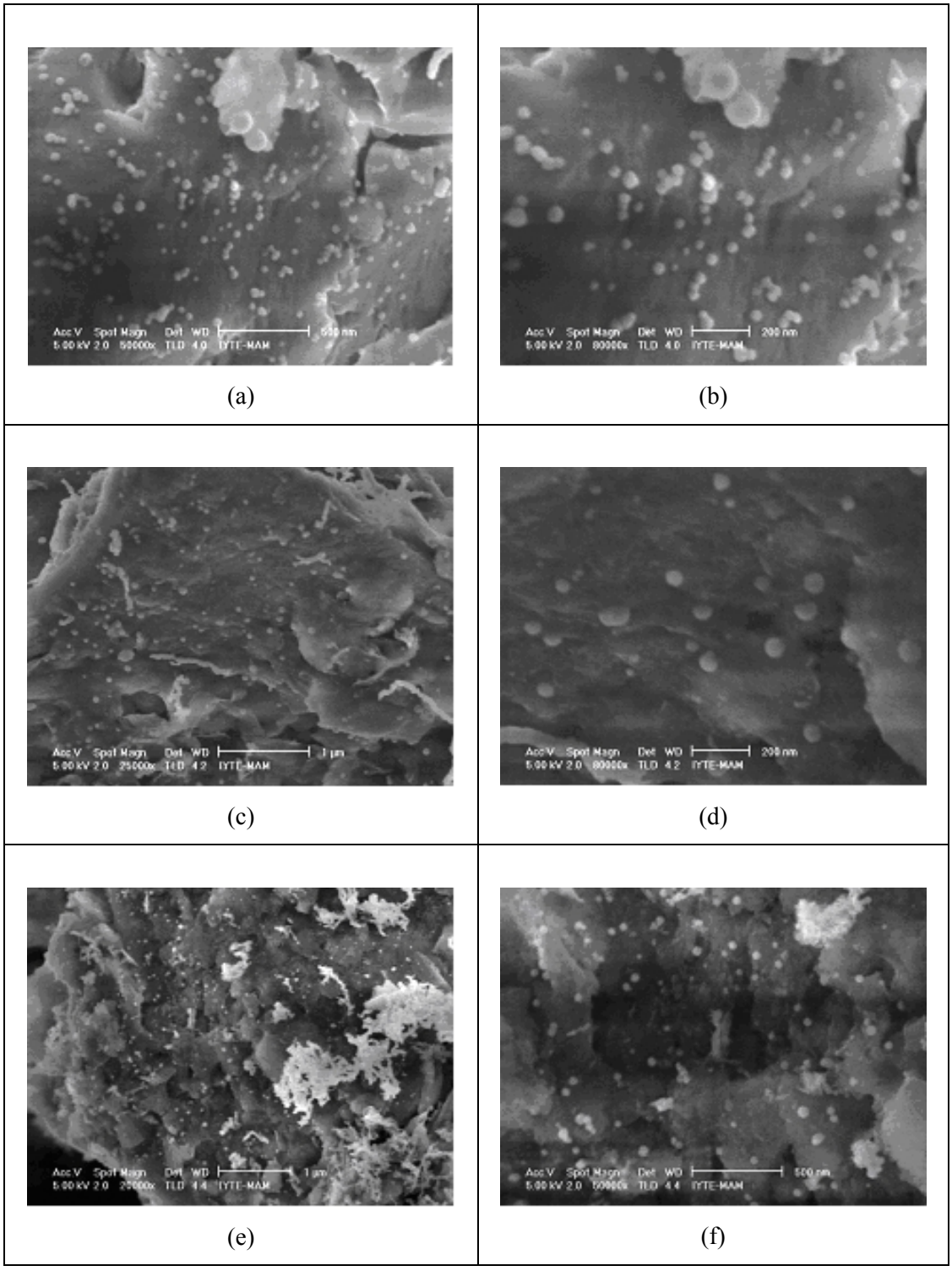

Figure 3.13. SEM images of mont-nZVI samples. (a) and (b) belong to 1:1, (c) and (d) 2:1, (e) and (f) 5:1 mont-nZVI.

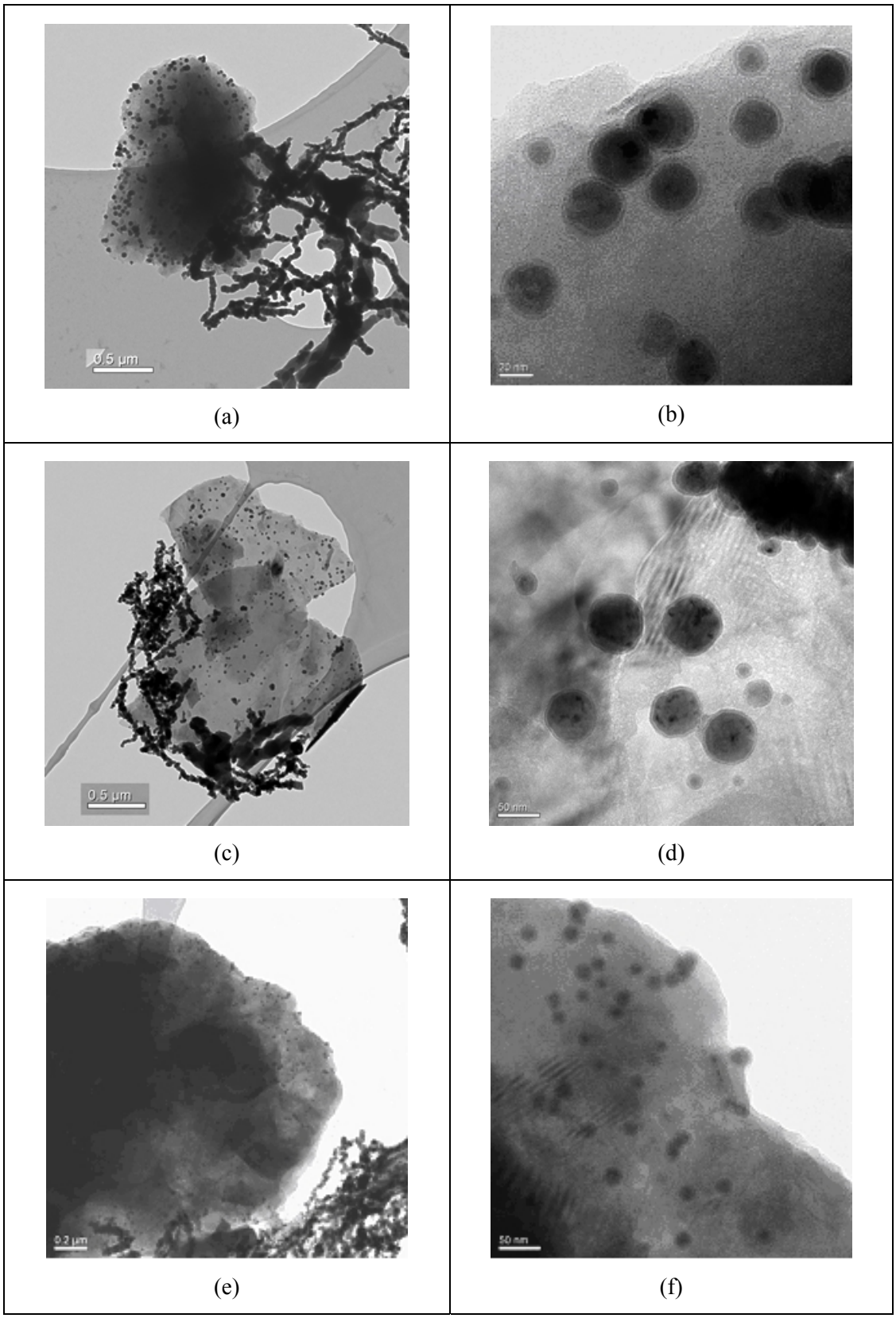

Figure 3.14. TEM images of mont-nZVI samples. (a) and (b) belong to 1:1, (c) and (d) 2:1, (e) and (f) 5:1 mont-nZVI.

3.2. Metal Uptake by Pure nZVI and Pure Clays

Prior to testing the synthesized kaol-nZVI and mont-nZVI as adsorbents for Co^{2+} and Cu^{2+} ions, the sorption capacity of pure nZVI, pure kaolinite and pure montmorillonite towards aqueous Co^{2+} and Cu^{2+} ions was investigated. These experiments formed a reference in the assessment of the sorption capacity of the synthezied new materials. For this purpose, batch tests were run with various initial metal concentrations as described in section 2.4.3. The findings are given in Table 3.3. and Table 3.4., and the resulting sorption isotherms are drawn in Figure 3.15

Generally the removal percentages decrease as the initial metal concentrations are increased for Co^{2+} and Cu^{2+} uptake. It is clear that nZVI shows greater removal capacities for Co^{2+} and Cu^{2+} in comparison to kaolinite and montmorillonite. The sorption capacity, within the studied concentration range of Co^{2+}, are 115 mg/g, 0.8 mg/g and 3 mg/g on nZVI, kaolinite, and montmorillonite, respectively. In the case of Cu^{2+} the corresponding sorption capacies are 180 mg/g, 8 mg/g and 16 mg/g on nZVI, kaolinite and montmorillonite, respectively.

Table 3.3. The equilibrium values corresponding to the uptake of Co^{2+} ions by nZVI, kaolinite and montmorillonite samples for various initial metal concentrations

	nZVI			Kaolinite			Montmorillonite		
$[Co^{2+}]_0$ (mg/L)	$[Co^{2+}]_l$ (mg/L)	$[Co^{2+}]_s$ (mg/g)	% Sorption	$[Co^{2+}]_l$ (mg/L)	$[Co^{2+}]_s$ (mg/g)	% Sorption	$[Co^{2+}]_l$ (mg/L)	$[Co^{2+}]_s$ (mg/g)	% Sorption
500	354.00	116.80	29	495.00	4.00	1	499.00	0.80	0
250	119.00	104.80	52	246.50	2.80	1	249.50	0.40	0
100	0.60	79.52	99	96.26	2.99	4	97.60	1.92	2
50	0.10	39.92	100	48.60	1.12	3	49.00	0.80	2
10	0.00	8.00	100	9.76	0.19	2	6.76	2.59	32
5	0.01	3.99	100	4.51	0.39	10	2.36	2.11	53
1	0.16	0.67	84	0.63	0.30	37	0.28	0.58	72

Table 3.4. The equilibrium values corresponding to the uptake of Cu^{2+} ions by nZVI, kaolinite and montmorillonite samples for various initial metal concentrations

	nZVI			Kaolinite			Montmorillonite		
$[Cu^{2+}]_0$ (mg/L)	$[Cu^{2+}]_l$ (mg/L)	$[Cu^{2+}]_s$ (mg/g)	% Sorption	$[Cu^{2+}]_l$ (mg/L)	$[Cu^{2+}]_s$ (mg/g)	% Sorption	$[Cu^{2+}]_l$ (mg/L)	$[Cu^{2+}]_s$ (mg/g)	% Sorption
500	258	193.6	48	490	8	2	480	16	4
250	42	166.4	83	240	8	4	232.5	14	7
100	7.8	73.76	92	93.6	5.12	6	83.6	13.12	16
50	3.5	37.2	93	44.3	4.56	11	39	8.8	22
10	1.35	6.92	87	9.08	0.736	9	6.06	3.152	39
5	0.79	3.368	84	4	0.8	20	2.35	2.12	53
1	0.1	0.72	90	0.61	0.312	39	0.22	0.624	78

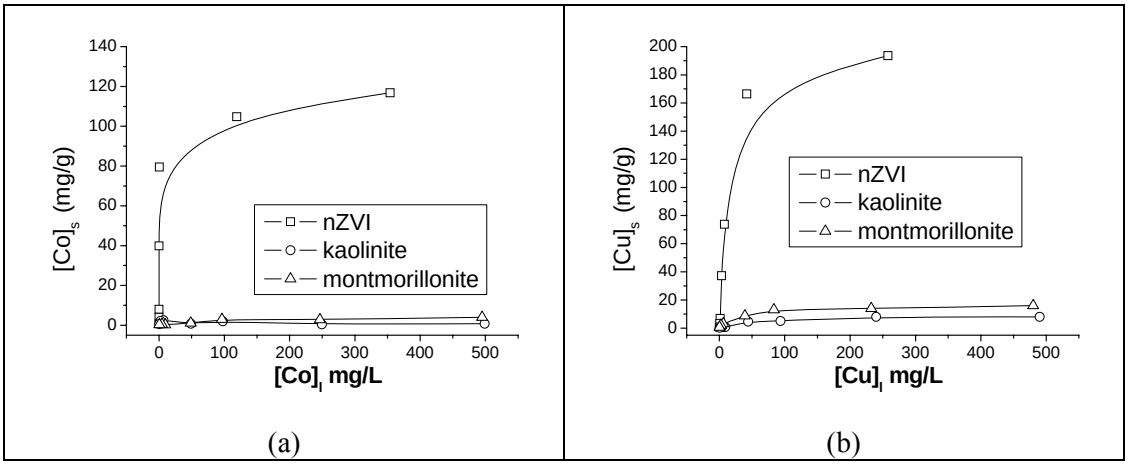

Figure 3.15. Sorption isotherms of (a) Co^{2+} and (b) Cu^{2+} obtained by contact of the ions with nZVI, kaolinite and montmorillonite samples

3.3. Metal Uptake by Kaolinite-nZVI

In this part of the study, kaolinite-supported nZVI was applied in the sequestration of Co^{2+} and Cu^{2+} ions under different experimental conditions. The results of the experiments are provided in the corresponding subsections below.

3.3.1. V/m Ratio Experiments

Metal removal trends with respect to (volume of metal solution)/(mass of sorbent) were studied under the conditions given in section 2.4.1. Throughout this work, the values of %Sorption were calculated for Co^{2+} and Cu^{2+} ions using the formula:

$$\%\text{Sorption} = \frac{[M]_o - [M]_l}{[M]_o} \times 100\%$$

In this formula, $[M]_0$ and $[M]_l$ are the initial and the equilibrium ion concentrations in mg/L respectively. The equilibrium ion concentration on the solid phase, $[M]_s$ (mmol/g), was calculated by the formula:

$$[M]_S = \frac{[M]_0 - [M]_l}{MW_{metal}} \times \frac{V}{m}$$

where MW_{metal} is the molecular weight of metal (g/mol), V is the solution volume (L) and m is the sorbent mass (g). Results are given in tables below.

Table 3.5. The equilibrium values corresponding to the uptake of Co^{2+} ions by 5:1 kaol-nZVI sample at various V/m ratios (mass of sorbent: 0.05 g)

5:1 kaol-nZVI				
V/m (mL/g)	$[Co^{2+}]_0$ (mg/L)	$[Co^{2+}]_l$ (mg/L)	$[Co^{2+}]_s$ (mg/g)	% Sorption
200	50	1.40	9.72	97
	500	359.00	28.2	28
400	50	1.40	19.44	97
	500	416.00	33.6	17
600	50	5.90	26.46	88
	500	455.50	26.7	9
800	50	359.00	26.4	28
	500	459.50	32.4	8

Table 3.6. The equilibrium values corresponding to the uptake of Cu^{2+} ions by 5:1 kaol-nZVI sample at various V/m ratios (mass of sorbent: 0.05 g)

5:1 kaol-nZVI				
V/m (mL/g)	$[Cu^{2+}]_0$ (mg/L)	$[Cu^{2+}]_l$ (mg/L)	$[Cu^{2+}]_s$ (mg/g)	% Sorption
200	50	0.60	9.8	99
	500	254.00	48.4	49
400	50	1.10	19.52	98
	500	393.00	47.6	21
600	50	1.00	29.22	98
	500	413.50	52.5	17
800	50	254.00	25.6	49
	500	459.00	57.2	8

The removal of Co^{2+} and Cu^{2+} ions at an initial level of 50 mg/L appears to be quantitative up to V/m ratio of 600 mL/g by 5:1 kaol-nZVI. As expected, removal percentages increase as V/m ratio decreases. This trend shows that large amounts of Co^{2+} and Cu^{2+} can be removed form aqueous media by decreasing the V/m ratio, in other words by increasing the adsorbent amount per volume of solution.

3.3.2. Kinetic Experiments

Kinetic experiments were performed for 1:1, 2:1 and 5:1 kaol-nZVI samples as described in section 2.4.2. These studies indicate that kaol:nZVI synthesized at the ratios of 1:1, 2:1 and 5:1 clay:nZVI ratios have a capacity to remove Co^{2+} and Cu^{2+} from aqueous media with very fast kinetics. The variation of the sorbed amounts of Co^{2+} and Cu^{2+} ions on kaol-nZVI with time are given in Figure 3.16. For both ions, Co^{2+} and Cu^{2+}, the uptake process approaches equilibrium within 30 minutes, regardless of kaol:nZVI ratio. The equilibrium Co^{2+} concentrations on 1:1, 2:1 and 5:1 kaol-nZVI species were determined as 0.61, 0.50 and 0.46 mmol/g (36, 27 and 28 mg/g), respectively.

The equilibrium Cu^{2+} concentrations on 1:1 and 2:1 kaol-nZVI were found to be nearly the same, whereas Cu^{2+} concentration on 5:1 kaol-nZVI is much lower; 1.22, 1.22 and 0.42 mmol/g (78, 78 and 27 mg/g), respectively. This behavior is possibly

related with the different mechanisms of Co^{2+} and Cu^{2+} uptake by kaol-nZVI species, the thing that is considered later in this text.

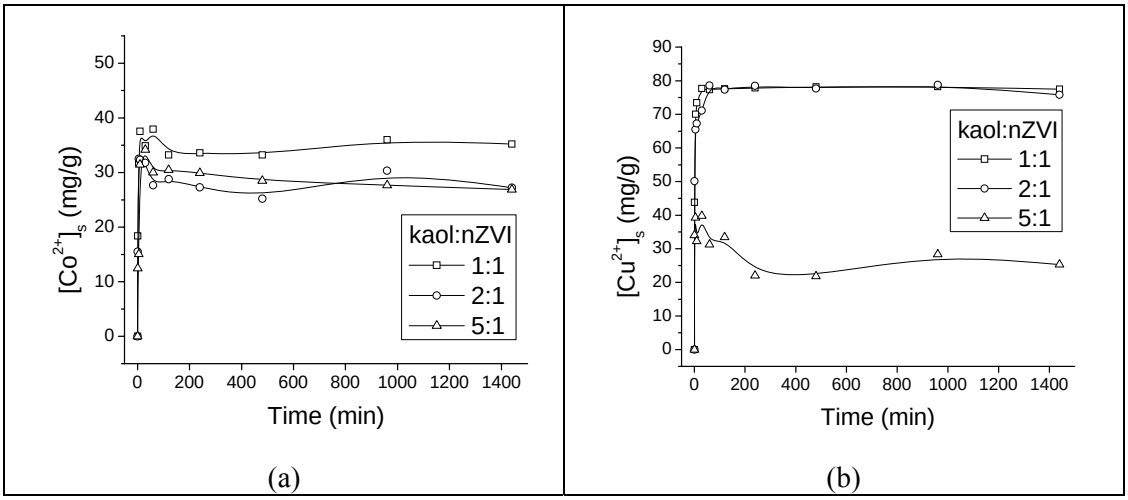

Figure 3.16. (a) Co^{2+} and (b) Cu^{2+} uptake on 1:1, 2:1 and 5:1 kaol-nZVI by time

3.3.3. Effect of Initial Metal Concentration

The variation in the extent of sorption of 1:1, 2:1 and 5:1 kaol-nZVI with different initial concentrations of Co^{2+} and Cu^{2+} ions were studied at the conditions described in section 2.4.3. The obtained equilibrium concentrations and %sorption values are given in Table 3.7 and Table 3.8 for Co^{2+} and Cu^{2+}, respectively, and the sorption isotherms are plotted in Figure 3.17. Based on the equilibrium values given in Table 3.7, it is apparent that up to an the initial concentration of 10 mg/L (V/m= 800 mL/g) quantitative removal of aqueous Co^{2+} ions can be achieved by all kaol-nZVI samples. The removal percentages decrease as the initial metal concentration is increased for all kaol-nZVI sorbents, the thing that points to an increase in the sorption barrier with loading. The equilibrium Co^{2+} concentration on the sorbents came out to be nearly the same (~25 mg/g). The observation that 5:1 kaol-nZVI is demonstrating a performance close to that of 1:1 and 2:1 kaol-nZVI could be related with better dispersion presumably associated with using lower Fe amounts at the stage of synthesis.

Table 3.7. The equilibrium values corresponding to the uptake of Co^{2+} ions by 1:1, 2:1 and 5:1 kaol-nZVI samples for various initial metal concentrations

kaol:nZVI	1:1			2:1			5:1		
$[Co]_0$ (mg/L)	$[Co]_l$ (mg/L)	$[Co]_s$ (mg/g)	% Sorption	$[Co]_l$ (mg/L)	$[Co]_s$ (mg/g)	% Sorption	$[Co]_l$ (mg/L)	$[Co]_s$ (mg/g)	% Sorption
500	469.00	24.80	6	468.00	25.60	6	460.00	25.60	6
250	231.50	22.80	11	215.50	27.60	14	220.50	23.60	12
100	70.70	23.44	29	72.20	22.24	28	69.60	24.32	30
50	32.45	14.04	35	32.10	14.32	36	18.10	25.52	64
10	0.28	7.78	97	0.21	7.83	98	0.47	7.62	95
5	0.33	3.74	93	0.37	3.70	93	0.19	3.85	96
1	0.10	0.72	90	0.09	0.73	91	0.10	0.72	90

Table 3.8. The equilibrium values corresponding to the uptake of Cu^{2+} ions by 1:1, 2:1 and 5:1 kaol-nZVI samples for various initial metal concentrations

kaol:nZVI	1:1			2:1			5:1		
$[Cu]_0$ (mg/L)	$[Cu]_l$ (mg/L)	$[Cu]_s$ (mg/g)	% Sorption	$[Cu]_l$ (mg/L)	$[Cu]_s$ (mg/g)	% Sorption	$[Cu]_l$ (mg/L)	$[Cu]_s$ (mg/g)	% Sorption
500	355.50	115.60	29	406.50	74.80	19	486.50	28.00	7
250	70.75	136.00	68	120.50	103.60	52	211.75	30.60	15
100	2.00	78.40	98	2.10	78.32	98	52.70	37.84	47
50	1.70	38.64	97	1.80	38.56	96	2.40	38.08	95
10	0.46	7.63	95	0.39	7.69	96	0.44	7.65	96
5	0.15	3.88	97	0.22	3.82	96	0.24	3.81	95
1	0.05	0.76	95	0.04	0.77	96	0.06	0.75	94

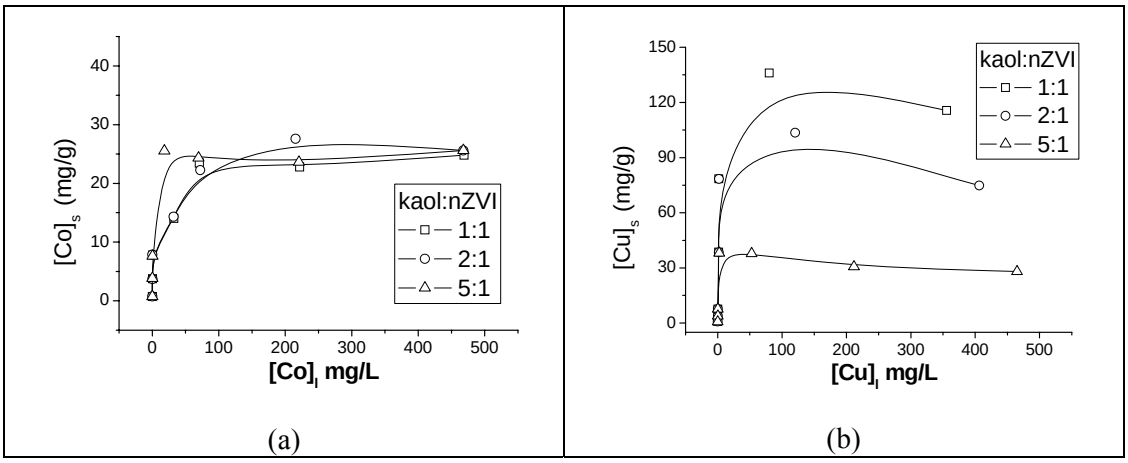

Figure 3.17. Sorption isotherms of (a) Co^{2+} and (b) Cu^{2+} obtained by contact of the ions with 1:1, 2:1 and 5:1 kaol-nZVI samples

On the other hand, the equilibrium concentrations given in Table 3.8 show that 1:1 and 2:1 kaol-nZVI samples are capable of removing Cu^{2+} almost completely up to an initial concentration of 100 mg/L, while 5:1 kaol-nZVI can achieve a nearly total removal of Cu^{2+} up to an initial concentration of 50 mg/L at the studied V/m ratio, 800 mL/g. The removal percentages decrease as the initial Cu^{2+} concentration is increased. Unlike the Co^{2+} case, equilibrium Cu^{2+} concentrations on the sorbents decreases as the nZVI ratio decreases in kaol-nZVI composites. The sorption capacity values are ~120 mg/g, ~90 mg/g and ~40 mg/g for 1:1, 2:1 and 5:1 kaol-nZVI, respectively. As discussed within the context of sorption mechanism later in this text (section 3.6), Cu^{2+} is removed mainly via a redox mechanism, and the amount of nZVI seems to surpass the effect of dispersion on the extent of removal of Cu^{2+} ions by kaol-nZVI material. In general, the removal percentages for Cu^{2+} appear to be higher than those for Co^{2+}. Several factors like ionic radii of ions, different standard reduction potentials and consequently different uptake mechanisms might be responsible for the observed removal trends.

3.3.4. Effect of pH

The effect of initial pH of metal solutions on sorption capacity was studied using 5:1 kaol-nZVI sample as described in section 2.4.4. Initial equilibrium metal concentrations in liquid and solid in addition to %Sorption are given at different initial pH values in Table 3.9 for Co^{2+} and in Table 3.10 for Cu^{2+} ions.

Table 3.9. The equilibrium values corresponding to the uptake of Co^{2+} ions by 5:1 kaol-nZVI at various initial pH values

pH	$[Co^{2+}]_0$ (mg/L)	$[Co^{2+}]_l$ (mg/L)	$[Co^{2+}]_s$ (mg/g)	% Sorption
4.00	100	43.30	45.36	57
6.00	100	39.15	48.68	61
8.00	100	19.05	64.76	81
10.00	100	1.95	78.44	98

Table 3.10. The equilibrium values corresponding to the uptake of Cu^{2+} ions by 5:1 kaol-nZVI at various initial pH values

pH	$[Cu^{2+}]_0$ (mg/L)	$[Cu^{2+}]_l$ (mg/L)	$[Cu^{2+}]_s$ (mg/g)	% Sorption
4.00	100	35.65	51.48	64
6.00	100	18.45	65.24	82
8.00	100	2.00	78.4	98
10.00	100	1.15	79.08	99

The values of equilibrium concentrations and %sorption show that the removal percentages of both of Co^{2+} and Cu^{2+} ions increase as the initial pH of the metal solutions increase. As the pH increases, insoluble hydroxides of these metals could arise, the thing that enhances their removal. On the contrary, the lower removal percentages at low pH values can be explained by the strong electrostatic repulsions between the kaol-nZVI particles and the cationic metal ions. At low pH media, kaol-nZVI particles have high positive surface potentials (Figure 3.10) and hence high positive surface charges, the thing that causes repulsions with the cationic species of

Co^{2+} and Cu^{2+} in the solution. It worths noting that at all initial solution pH values, higher removal percentages are observed for Cu^{2+} compared to Co^{2+}.

3.3.5. Repetitive Applications

Since iron as a material is susceptible to oxidation upon exposure to environmental conditions, it is necessary to assess the reusability of this material as synthesized. The relevant experiments were performed using 5:1 kaol-nZVI under the experimental conditions outlined in section 2.4.5.

The obtained results are shown in Figure 3.18 in terms of the %sorption versus the number of applications at the initial concentrations of 5 and 100 mg/L of Co^{2+} and Cu^{2+}. The kaol-nZVI sample seems to be effective for more than 90% removal of Co^{2+} and Cu^{2+} at the initial concentration of 5 mg/L concentration level after 4-5 successive uses, respectively. When the applied metal concentration is increased to 100 mg/L, more than 90% removal of Co^{2+} is still possible after 2 uses and removal of Cu^{2+} is still possible after 3 uses of the same sorbent. Taking into account that the concentrations of the two ions in underground water and even in industrial wastewaters are usually much less than 100 mg/L, it can be stated that multiple usage of the material seems to be plausible.

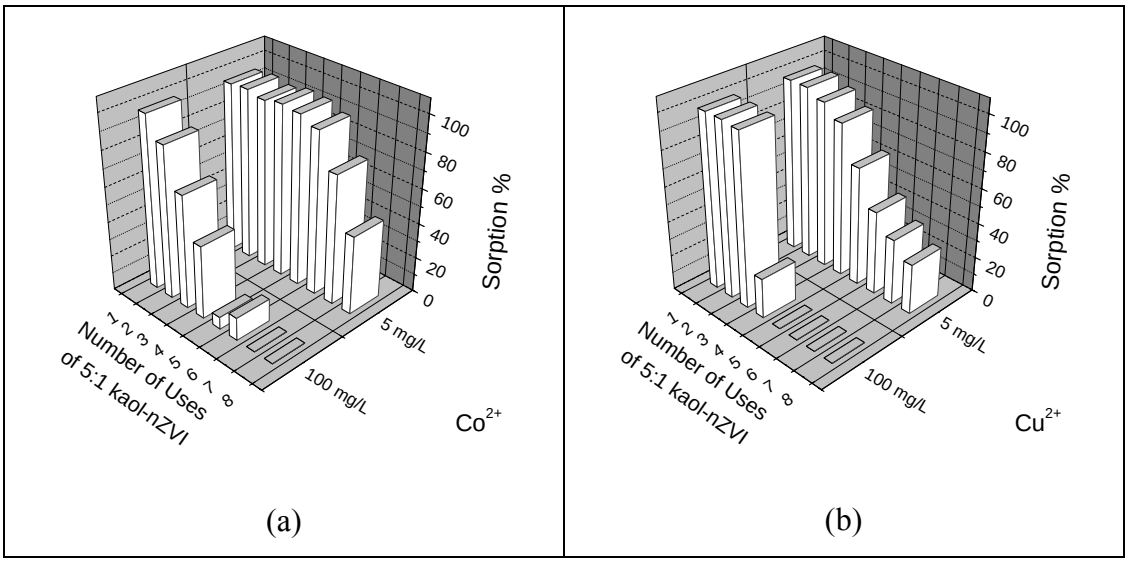

Figure 3.18. Variation of (a) Co^{2+} and (b) Cu^{2+} %Sorption with number of uses of 5:1 kaol-nZVI

3.4. Metal Uptake by Montmorillonite-nZVI

The experiments performed using kaolinite-supported nZVI were repeated using montmorillonite-supported nZVI (mont-nZVI) under identical experimental conditions. The results of the experiments are provided in the corresponding subsections below.

3.4.1. V/m Ratio Experiments

The relevant experiments were performed according to the conditions given in section 2.4.1. The calculations were made as described in part 3.3.1 for kaol-nZVI, and the results regarding Co^{2+} and Cu^{2+} uptake at various V/m ratios are given in Table 3.11 and Table 3.12, respectively. According to these results, nearly a complete removal of Co^{2+} ions at an initial concentration of 50 mg/L is possible at V/m ratios up to 600. At the same concentration, Cu^{2+} ions can be removed almost completely even at a V/m ratio of 800 mL/g. For both ions, the removal percentages increase as V/m ratio decreases, thus higher amounts of Co^{2+} and Cu^{2+} can be removed form aqueous media

by decreasing the V/m ratio, in other words by increasing the adsorbent amount per volume of solution.

Table 3.11. The equilibrium values corresponding to the uptake of Co^{2+} ions by 5:1 mont-nZVI sample at various V/m ratios

5:1 mont-nZVI				
V/m (mL/g)	$[Co^{2+}]_0$ (mg/L)	$[Co^{2+}]_l$ (mg/L)	$[Co^{2+}]_s$ (mg/g)	% Sorption
200	50	1.00	9.8	98
	500	258.00	48.4	48
400	50	1.20	19.52	98
	500	381.00	47.6	24
600	50	1.30	29.22	97
	500	412.50	52.5	18
800	50	18.00	25.6	64
	500	428.50	57.2	14

Table 3.12. The equilibrium values corresponding to the uptake of Cu^{2+} ions by 5:1 mont-nZVI sample at various V/m ratios

5:1 mont-nZVI				
V/m (mL/g)	$[Cu^{2+}]_0$ (mg/L)	$[Cu^{2+}]_l$ (mg/L)	$[Cu^{2+}]_s$ (mg/g)	% Sorption
200	50	1.10	9.78	98
	500	210.50	57.9	58
400	50	1.80	19.28	96
	500	346.00	61.6	31
600	50	2.20	28.68	96
	500	425.50	44.7	15
800	50	1.80	38.56	96
	500	436.50	50.8	13

3.4.2. Kinetic Experiments

Kinetic experiments were performed for 1:1, 2:1 and 5:1 mont-nZVI samples as described in section 2.4.2. The results are drawn in Figure 3.19 in terms of the variation of the sorbed amount of metal (Co^{2+} or Cu^{2+}) on mont-nZVI surface with time. According to these results, 1:1, 2:1 and 5:1 mont-nZVI can remove Co^{2+} and Cu^{2+} from aqueous media with relatively fast kinetics. In the case of Co^{2+}, the uptake process approaches equilibrium in about an hour regardless of mont:nZVI ratio. At the studied concentration, the equilibrium Co^{2+} concentrations on 1:1, 2:1 and 5:1 kaol-nZVI materials were determined as 0.49, 0.64 and 0.44 mmol/g (28, 38 and 27 mg/g), respectively.

In comparison to the uptake of Co^{2+}, the uptake of Cu^{2+} takes more time to come to equilibrium; about four hours for 1:1 and 2:1 mont:nZVI. In the case of 5:1 mont:nZVI, the equilibrium ion concentration on the sorbent seems to continue to slightly increase even after 24 hours of mixing, but the change is not significant (Figure 3.19). The concentrations of Cu^{2+} on the sorbents was determined as 0.70, 1.01 and 0.91 mmol/g (45, 64 and 58 mg/g), respectively.

Longer time seems to be necessary to approach equilibrium in the case of mont-nZVI in comparison to kaol-nZVI, particularily in the case of Cu^{2+}. The longer sorption time on mont-nZVI might be attributed to the difference in structural properties of kaolinite and montmorillonite. In kaolinite case, the interlayer space is not accessible, and as a result most of the nZVI particles are present on the easily accessible outer surface and edge parts of the clay. Montmorillonite, however, is known for its larger interlayer space and its interlayer sites are responsible for the high surface area of the clay. Thus, for the sorbates to reach nZVI particles in the interlayer space ,they must first overcome the diffusion barrier of the interlayer part.

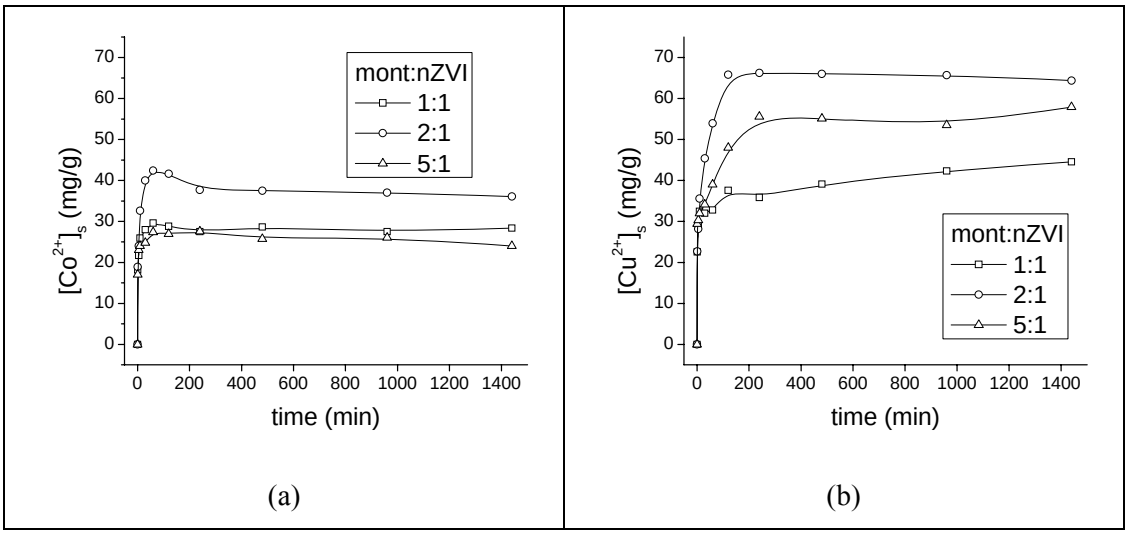

Figure 3.19. (a) Co^{2+} and (b) Cu^{2+} uptake on 1:1, 2:1 and 5:1 mont-nZVI by time

3.4.3. Effect of Initial Metal Concentration

The values of equilibrium concentrations and %sorption for Co^{2+} uptake on 1:1, 2:1 and 5:1 mont-nZVI samples are given in Table 3.13. The extent of removal decreases as the initial metal concentration is increased for all mont-nZVI sorbents. The results indicate that the quantitative removal of Co^{2+} from aqueous media is possible up to an initial concentration of 10 mg/L at the studied volume/mass ratio, 800 mL/g. In line with the trend observed for kaol-nZVI, the amount of sorbed Co^{2+} is nearly the same for 1:1, 2:1 and 5:1 mont-nZVI (~35 mg/g). Like in the case of kaol-nZVI, this result might be explained on the basis of a presumable better enhancement in the dispersion of nZVI particles as the quantity of Fe^{2+} is decreased at the stage of mont-nZVI synthesis.

The values of equilibrium concentrations given in Table 3.14 mont-nZVI samples are capable of almost a complete removal of Cu^{2+} ions up to an initial concentration of 50 mg/L at the studied V/m ratio, 800 mL/g. The removal percentages decrease as the initial Cu^{2+} concentration is increased. Unlike the Co^{2+} case, equilibrium Cu^{2+} concentrations on the sorbents show some variation with the change in the nZVI amount in the mont-nZVI materials. In general, the removal percentages for Cu^{2+} are

higher than those for Co^{2+}, like in the case of kaol-nZVI (section 3.3.3.). Sorption isotherms are given in Figure 3.20.

Table 3.13. The equilibrium values corresponding to the uptake of Co^{2+} ions by 1:1, 2:1 and 5:1 mont-nZVI samples for various initial metal concentrations

mont:nZVI	**1:1**			**2:1**			**5:1**		
$[Co^{2+}]_0$ (mg/L)	$[Co^{2+}]_l$ (mg/L)	$[Co^{2+}]_s$ (mg/g)	% Sorption	$[Co^{2+}]_l$ (mg/L)	$[Co^{2+}]_s$ (mmol/g)	Sorption %	$[Co^{2+}]_l$ (mg/L)	$[Co^{2+}]_s$ (mg/g)	% Sorption
500	452.50	38.00	9	450.00	40.00	10	437.50	50.00	13
250	198.50	41.20	21	195.00	44.00	22	199.50	40.40	20
100	67.90	25.68	32	56.30	34.96	44	65.40	27.68	35
50	19.40	24.48	61	14.40	28.48	71	18.05	25.56	64
10	0.42	7.66	96	0.45	7.64	96	0.20	7.84	98
5	0.33	3.74	93	0.39	3.69	92	0.15	3.88	97
1	0.16	0.67	84	0.09	0.73	91	0.07	0.74	93

Table 3.14. The equilibrium values corresponding to the uptake of Cu^{2+} ions by 1:1, 2:1 and 5:1 mont-nZVI samples for various initial metal concentrations

mont:nZVI	**1:1**			**2:1**			**5:1**		
$[Cu^{2+}]_0$ (mg/L)	$[Cu^{2+}]_l$ (mg/L)	$[Cu^{2+}]_s$ (mg/g)	% Sorption	$[Cu^{2+}]_l$ (mg/L)	$[Cu^{2+}]_s$ (mgl/g)	% Sorption	$[Cu^{2+}]_l$ (mg/L)	$[Cu^{2+}]_s$ (mg/g)	% Sorption
500	453.50	37.20	9	436.00	51.20	13	451.00	39.20	10
250	184.25	52.60	26	162.75	69.80	35	193.50	45.20	23
100	37.00	50.40	63	14.00	68.80	86	32.00	54.40	68
50	2.05	38.36	96	1.35	38.92	97	1.95	38.44	96
10	0.72	7.42	93	1.38	6.90	86	1.12	7.10	89
5	0.50	3.60	90	0.79	3.37	84	0.65	3.48	87
1	0.16	0.67	84	0.24	0.61	76	0.06	0.75	94

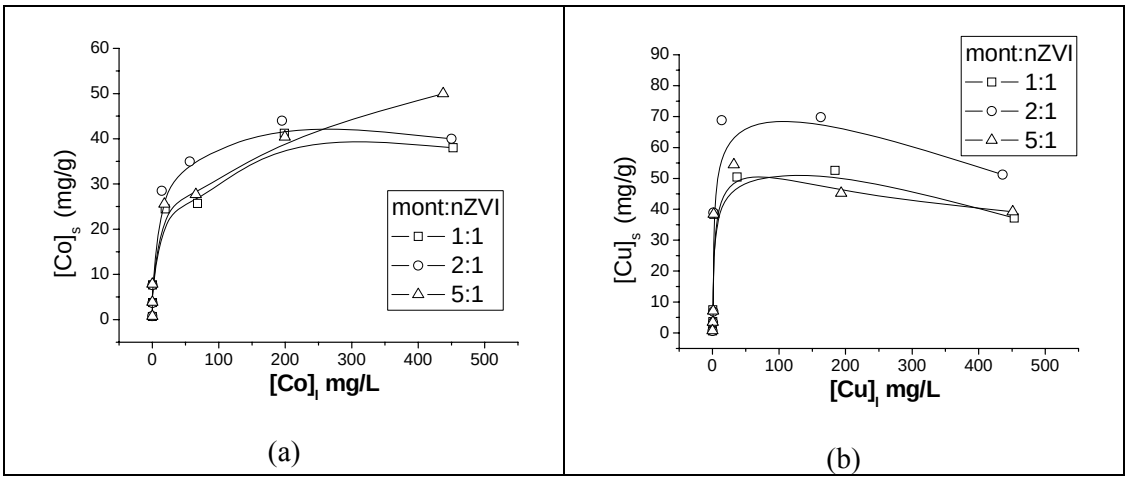

Figure 3.20. Sorption isotherms of (a) Co^{2+} and (b) Cu^{2+} obtained by contact of the ions with 1:1, 2:1 and 5:1 mont-nZVI samples

3.4.4. Effect of pH

To study the effect of initial pH of metal solutions on the sorption capacity of 5:1 mont-nZVI, batch experiments were run as described in accordance with the experimental conditions given in section 2.4.4. The obtained equilibrium metal concentrations in the liquid and on the solid, in addition to the corresponding %sorption values are provided in Table 3.15 and Table 3.16 for Co^{2+} and Cu^{2+} ions, respectively. The results show that the removal percent of both of Co^{2+} and Cu^{2+} ions increase as the initial pH of the metal solutions increase. The possible sources of this behavior were discussed in section 3.3.4.

Table 3.15. The equilibrium values corresponding to the uptake of Co^{2+} ions by 5:1 mont-nZVI at various initial solution pH values

pH	$[Co^{2+}]_0$ (mg/L)	$[Co^{2+}]_l$ (mg/L)	$[Co^{2+}]_s$ (mmol/g)	% Sorption
4.00	100	50.7	39.44	49
6.00	100	43.5	45.2	57
8.00	100	28.7	57.04	71
10.00	100	11.6	70.72	88

Table 3.16. The equilibrium values corresponding to the uptake of Cu^{2+} ions by 5:1 mont-nZVI at various initial solution pH values

pH	$[Cu^{2+}]_0$ (mg/L)	$[Cu^{2+}]_l$ (mg/L)	$[Cu^{2+}]_s$ (mmol/g)	% Sorption
4.00	100	37.5	50	63
6.00	100	13.6	69.12	86
8.00	100	5.6	75.52	94
10.00	100	9.5	72.4	91

3.4.5. Repetitive Applications

The reusability of 5:1 mont-nZVI for the removal of Co^{2+} and Cu^{2+} was tested under the conditions given in section 2.4.5. The results are shown in Figure 3.21 in terms of the values of %sorption obtained at successive trials of the sorbent at the initial concentrations of 5 and 100 mg/L of Co^{2+} and Cu^{2+}. The sorbent appears to be effective for quantitative removal of Co^{2+} and Cu^{2+} at 5 mg/L concentration level even after 8 successive uses of the same sorbent. When the applied metal concentration is increased to 100 mg/L, more than 90% removal of Co^{2+} is still possible after 3 uses and a similar removal of Cu^{2+} can be achieved even after 4 uses of the same sorbent. As was mentioned in section 3.3.5., taking into account that the concentrations of the two ions in underground water and even in industrial wastewaters are usually much less than 100 mg/L, it can be stated that multiple usage of the material seems to be plausible.

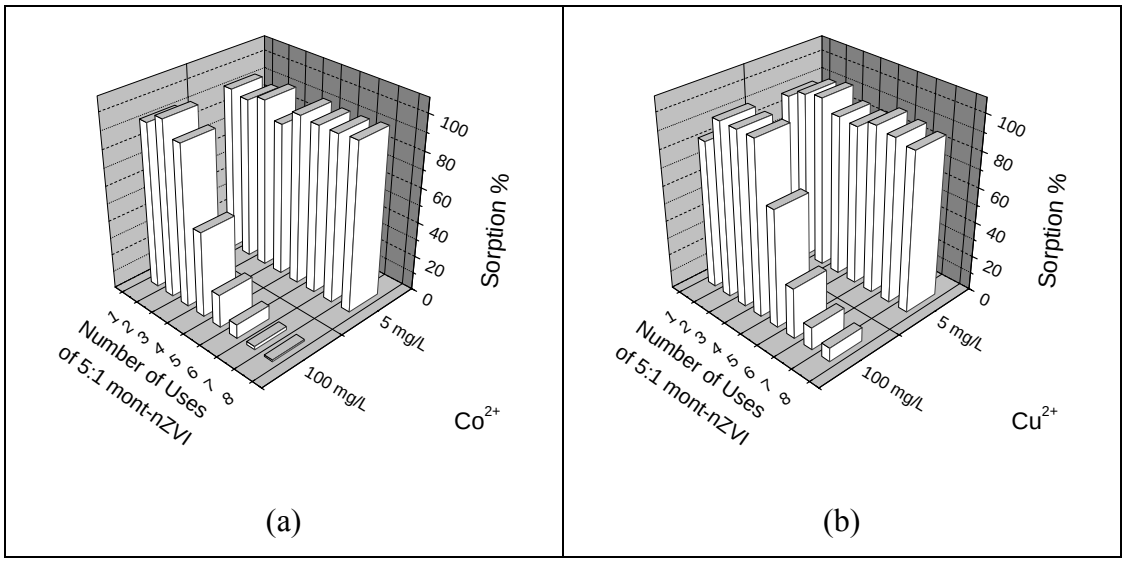

Figure 3.21. Variation of (a) Co^{2+} and (b) Cu^{2+} %Sorption with number of uses of 5:1 mont-nZVI

3.5. Comparative Evaluation of kaol-nZVI and mont-nZVI as Sorbents

Considering the differences in structure and physical properties of kaolinite and montmorillonite in aqueous media, one can predict that these differences will be reflected on the performance of kaol-nZVI and mont-nZVI as sorbents.

In general, kaol-nZVI samples were observed to remove both Co^{2+} and Cu^{2+} with faster kinetics in comparison to mont-nZVI samples. The longer sorption time on mont-nZVI might be attributed to the difference in structural properties of kaolinite and montmorillonite. In kaolinite case, the interlayer space is not accessible, and as a result most of the nZVI particles are present on the easily accessible outer surface and edge parts of the clay. Montmorillonite, however, is known for its larger interlayer space and its interlayer sites are responsible for the high surface area of the clay. Thus, for the sorbates to reach nZVI particles in the interlayer space they must first overcome the diffusion barrier of the interlayer part, thus requiring relatively longer time to undergo the intrinsic sorption step,

Considering the sorption capacity, within the studied conditions, the equilibrium Co^{2+} concentrations on mont-nZVI samples (~35 mg/g) are larger than the equilibrium Co^{2+} concentrations on kaol-nZVI samples (~25 mg/g), in other words mont-nZVI

samples are better sorbents in terms of the total amount of sorbed Co^{2+} ions. Interestingly, the retardation of Cu^{2+} is achieved more effectively by applying kaol-nZVI samples in comparison with mont-nZVI samples. The concentration of Cu^{2+} on mont-nZVI sorbents ranges from 45 mg/g to 60 mg/g, while the sorption capacity of kaol-nZVI could reach up to 120 mg/g. More work is still required to verify these results.

A notable behavior of Co^{2+} and Cu^{2+} uptakes by kaol-nZVI and mont-nZVI is that, Co^{2+} uptake capacity seems to be nearly independent on the clay:iron ratio both for kaolinite- and montmorillonite-supported iron nanoparticles at the studied clay:iron ratios. For Cu^{2+} retardation however, the amount of zero-valent iron in clay-supported materials seems to affect the extent of uptake capacity. This observation might be related from one side with the extent of dispersion of nZVI on the clay; presumably better dispersion at lower starting Fe^{2+} concentration at the stage of synthesis, the thing that enhances the fixation ability of the clay-nZVI material as a result of increasing the surface reactivity. From the other side, lowering the amount of Fe in the clay-nZVI composite will decrease the reduction ability of the sorbent towards the sorbate. Thus, the trend observed for a given sorbate seems to be closely related with particular sorption mechanism of that sorbate, i.e. whether the mechanism is dominated by a redox process or just electrostatic and/or surface complexation. The uptake mechanisms of Co^{2+} and Cu^{2+} on zero-valent iron surface are discussed in section 3.6.

In order to demonstrate the potential of the synthesized materials as sorbents for Co^{2+} and Cu^{2+} ions, the obtained sorption capacities in this study were compared with those provided in literature for other common sorbents. The data are given in Table 3.17 and Table 3.18 for Co^{2+} and Cu^{2+} uptake, respectively. At this point it should be stressed that experimental conditions may vary between the relevant studies and the comparison made here aims at demonstrating the uptake potential of clay supported iron nanoparticles rather than establishing a quantitative scale of efficacy among different sorbents.

Table 3.17. A comparison of Co^{2+} uptake capacities by different sorbent materials

Sorbent	Uptake Capacity mg/g	Reference
nZVI	115.0	This Study
Kaolinite	0.8	This Study
kaol-nZVI 1:1	25	This Study
kaol-nZVI 2:1	25	This Study
kaol-nZVI 5:1	25	This Study
Montmorillonite	3	This Study
mont-nZVI 1:1	35	This Study
mont-nZVI 2:1	35	This Study
mont-nZVI 5:1	35	This Study
Activated carbon	13.88	Demirbas 2003
Vermiculite	49.49	Da Fonseca, et al. 2005
IRN77 resin	86.17	Rengaraj and Moon 2002
Anaerobic granular sludge	18.76	van Hullebusch, et al. 2006
Hydroxyapatite	20.19	Smičiklas, et al. 2006
TVEX–PHOR resin	8.7	El-Dessouky, et al. 2007

Table 3.18. A comparison of Cu^{2+} uptake capacities by different sorbent materials

Sorbent	Uptake Capacity mg/g	Reference
nZVI	180.0	This Study
Kaolinite	8	This Study
kaol-nZVI 1:1	120	This Study
kaol-nZVI 2:1	90	This Study
kaol-nZVI 5:1	40	This Study
Montmorillonite	16	This Study
mont-nZVI 1:1	45	This Study
mont-nZVI 2:1	60	This Study
mont-nZVI 5:1	45	This Study
Activated carbon	24.1	Chen and Wu 2004 *
Baggase fly ash	2.26	Gupta and Ali 2000 *
Groundnut shell	4.48	Shukla and Pai 2005 *
Kaolinite	16.9	Wang, et al. 2006b *
C. ranguformis	7.68	Ekmekyapar, et al. 2006 *
Cankırı bentonite	44.84	Veli and Alyüz 2007
Chitosan	139.8	Verbych, et al. 2005
** Provided from the table in Wang, et al. 2006b*		

3.6. The Uptake Mechanisms

As discussed in section 1.3, it was reported that nZVI has the ability to remove metal ions from aqueous solution by multiple mechanisms closely related on the core-shell structure of the nanoparticles (Li and Zhang 2007). These mechanisms include electrostatic adsorption, complex formation, reduction, and precipitation (Li and Zhang 2007). The standard reduction potential of Co^{2+} (= -0.28 V, 298 K) is somewhat larger than that of Fe^{2+} (= -0.44 V, 298 K), and it is theoretically worth to consider that the removal of Co^{2+} can be achieved by a redox reaction in which insoluble Co^0 is produced. In literature, there are some reports in which the oxidation-reduction mechanism was shown to be effective in the uptake of a number of ions that are higher in the electrochemical series than Fe^{2+} including Pb^{2+} and Cr(VI) (Ponder, et al. 2000), Ni^{2+} (Li and Zhang 2006), As (III) and As(V) (Kanel, et al. 2005 , Kanel, et al. 2006) and Cu^{2+}, Ni^{2+} and Ag^{+} (Li and Zhang 2007). However, XPS analysis of cobalt treated nZVI in this study did not confirm that sorbed cobalt was present in its zero-valent form. According to this analysis, Co $2p_{3/2}$ peaks are located at 781.2±0.1 eV and are asymmetric to the high binding energy side, as shown in Figure 3.23 (a). This value occurs amid the values reported earlier to correspond to Co^{2+} in CoO (780.0±0.2 eV for the $2p_{3/2}$ line) (McIntyre and Cook 1975, McIntyre, et al. 1990), and to Co^{2+} in $Co(OH)_2$ (782.0±0.1 eV for the $2p_{3/2}$ line) (Tan, et al. 1991). Both lines are readily distinguished from that corresponding to metallic cobalt, Co^0 (778.0±0.2 eV for the Co $2p_{3/2}$ line) (McIntyre and Cook 1975, Wagner, et al. 1979). Based on this, it can be suggested that Co^{2+} ions were not exposed to reduction upon their fixation by iron nanoparticles but were fixed by the oxohydroxyl groups at the surface of the shell of iron nanoparticles or simply precipitated on that surface in the form of $Co(OH)_2$. As reported earlier, iron nanoparticles form FeOOH groups on their surfaces when in contact with water as a result of surface hydroxylation and subsequent dehydration of the exposed shell (Li and Zhang 2007). The development of such groups is evident in the XPS spectrum provided in Figure 3.24 (a) for a sample of iron nanoparticles at the end of uptake. The recorded Fe 2p photoelectron profile was very similar to that attributed to Fe in ferrioxyhydroxide (FeOOH) with the Fe $2p_{3/2}$ line centered at 711.7±0.1 eV binding energy (Wagner, et al. 1979). The absence of Co^0 as a sorption product was also

confirmed by the XRD analysis which showed no signal that match with the basic reflections of metallic Co (Figure 3.22 (a)).

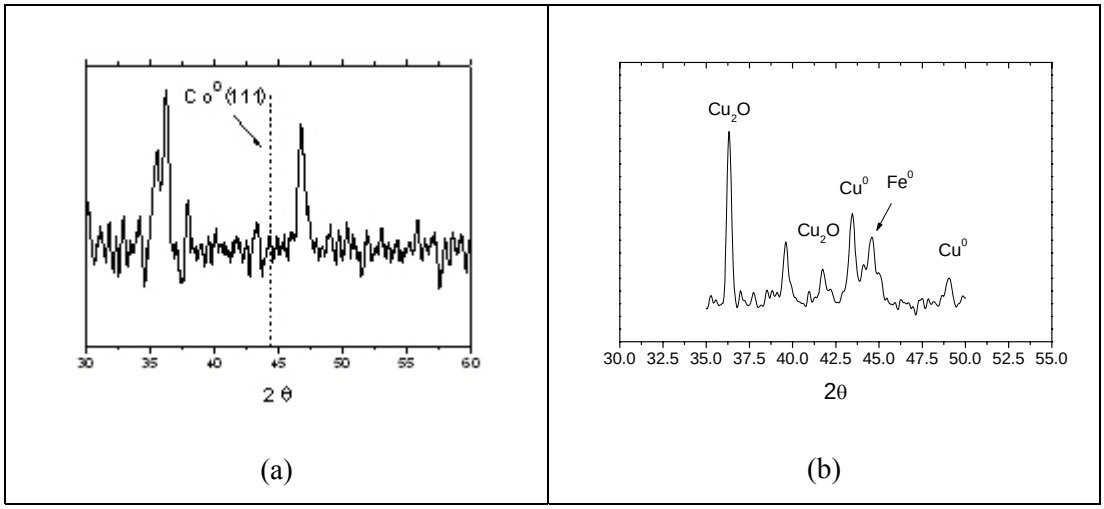

Figure 3.22. Powder XRD patterns of (a) Co^{2+} and (b) Cu^{2+} treated nZVI

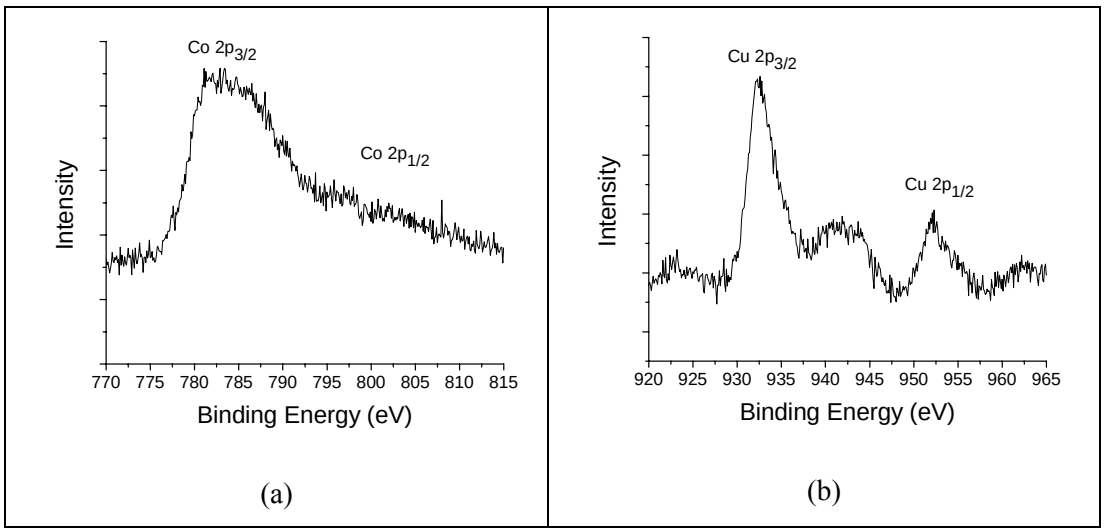

Figure 3.23. XPS spectra showing (a) Co peaks (b) Cu peaks for samples of iron nanoparticles at the end of mixing with Co^{2+} and Cu^{2+}

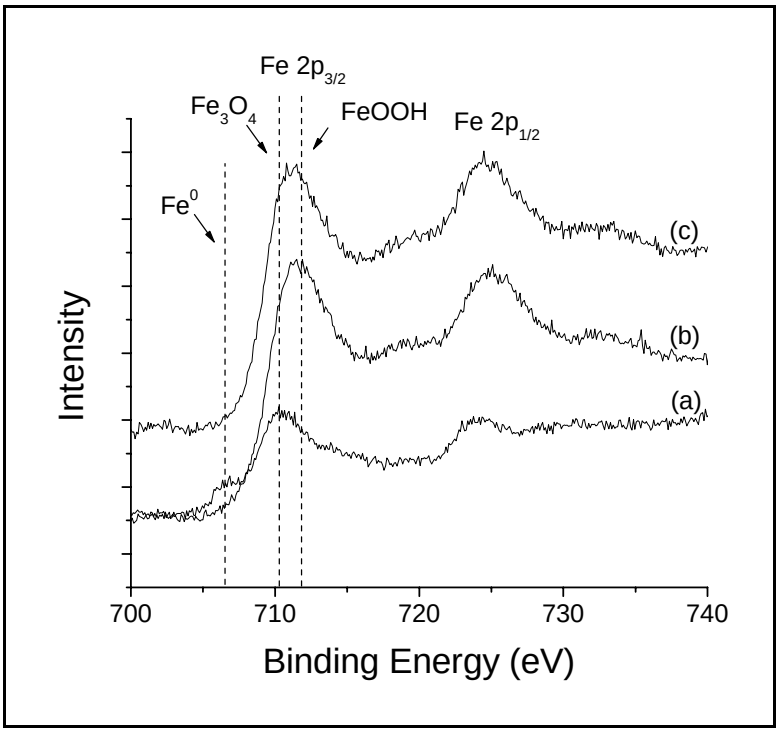

Figure 3.24. XPS spectra showing Fe peaks for: (a) an iron standard; and samples of iron nanoparticles after contact with (b) Co^{2+} and (c) Cu^{2+} aqueous solutions

The standard reduction potential of Cu^{2+} (=+0.34 V, 298 K) is well above that of Fe^{2+} (= -0.44 V, 298 K), so the uptake of Cu^{2+} ions would be expected to primarily take place via a redox mechanism. XPS analyses performed throughout this study have shown that Cu $2p_{3/2}$ lines were centred at a binding energy of 932.3±0.1 eV (Figure 3.23 (b)). In literature, the binding energy of metallic copper, Cu^0, is frequently reported for the Cu $2p_{3/2}$ line at 932.6±0.2 eV (Wagner 1975, Gaarenstroom 1977, Wagner, et al. 1979). Meanwhile, the binding energy reported for Cu^+ in Cu_2O is also very similar to that of the metal and is reported to be centred at 932.4±0.3 eV (Wagner 1975). However, by calculating the Auger parameter it is possible to determine the valence state of the Cu under analysis. The calculated Auger parameter indicated that the recorded signal was derived mainly from Cu^+ rather than Cu^0. These results agree in part with those reported recently by Zhang and Li (Li and Zhang 2007), who reported that Cu^{2+} ions are reduced to Cu^0 upon exposure to nZVI. However, they are in line with the finding of an earlier study in which ZVI in the scrap form was employed as an adsorbent of aqueous Cu^{2+} ions (Rangsivek and Jekel 2005). The recorded Fe 2p

photoelectron profile for Fe after contact with Cu^{2+} (Figure 3.24 (c)) was typical of that previously reported for Fe in hematite (Wagner, et al. 1979, Konno and Nagayama 1980, Paparazzo 1987) with the Fe $2p_{3/2}$ line centred at 711eV ±0.1eV binding energy.

The above findings are confirming that the primary adsorption mechanism is of redox type. The corresponding redox reactions, balanced by the standard redox method in acidic media, might be written as:

$$Fe^0 + Cu^{2+} \rightarrow Fe^{2+} + Cu^0$$

$$Fe^0 + 2Cu^{2+} + H_2O \rightarrow Fe^{2+} + Cu_2O + 2H^+$$

This result was also confirmed by XRD patterns recorded for iron nanoparticles at the end of the adsorption process. The XRD pattern presented in Figure 3.22 (b) is showing the appearance of a more intense signal of cuprite, Cu_2O compared to metallic copper, Cu^0.

CHAPTER 4

CONCLUSION

In this study, nanoscaled zero-valent iron (nZVI) (10-100 nm) was synthesized in ethanol by borohydride reduction method under atmospheric conditions. It was observed that iron nanoparticles are mainly in zero-valent oxidation state and that no significant oxidation took place for weeks of storage under atmospheric conditions. To enhance the removal effeciency and flexibility of the material in environmental applications, nZVI was supported by kaolinite and montmorillonite. Characterization of the clay-supported nZVI was performed using XRD, SEM/EDS, TEM, EELS, XPS, Zeta Meter, BET-N_2, and indicated partial dispersion of the chain-like structure of iron nanoparticles on the clay structure.

From the results of TEM and EELS, it was observed that iron nanoparticles consist of a zero-valent core and an oxide shell (3-5 nm thick) surrounding it, as previously reported in the literature. Unsupported iron nanoparticles tend to form chain like structures with a particle size in the range 20-80 nm, while clay supported iron nanoparticles exist mainly as dispersed nano spheres with radii within 10-50 nm. BET surface area of pure nZVI was determined as 14.19 m^2/g while this value ranges from 6.13 m^2/g to 9.55 m^2/g for kaol-nZVI materials, and from 34.82 m^2/g to 66.51 m^2/g for mont-nZVI materials. The iso-electric point (IEP) for nZVI was determined as 8.1. The IEP values for kaol-nZVI species were found about 7 and IEP values of mont-nZVI species were in the range 3-4.

The materials were then applied as sorbents for Co^{2+} and Cu^{2+} ions in aqueous media. According to results, unsupported and clay-supported nZVI has a great capacity to immobilize Co^{2+} and Cu^{2+} ions with very fast kinetics. In the case of kaol-nZVI, both Co^{2+} and Cu^{2+} uptake approach equilibrium within 30 minutes of contact time. In the case of mont-nZVI, which showed relatively slower kinetics, Co^{2+} and Cu^{2+} uptakes approached equilibium in 1 hour and 4 hours, respectively.

The obtained values of sorption capacities indicated that nearly the same amount of Co^{2+} removal is achievable with less iron content in kaol-nZVI and mont-nZVI species. This is seemingly related with the enhanced surface reactivity caused by better

dispersion at smaller Fe amounts, thus producing more FeOOH groups required for Co^{2+} fixation. For Cu^{2+} removal, however, the extent of sorption seems to correlate directly with the amount of nZVI in the composites, the thing possibly stemming from the redox nature of the sorption mechanism that leads to Cu^{2+} fixation as Cu_2O and Cu^0. The optimization of clay:nZVI in a manner that leads to maximizing the fixation of adsorbates remains a serious goal that requires extensive effort in future work.

The experiments performed with 5:1 kaol-nZVI and 5:1 mont-nZVI showed that more Co^{2+} and Cu^{2+} can be removed from aqueous media if the sorbent amount is increased. For both types of sorbents and for both ions under investigation, Co^{2+} and Cu^{2+}, it was determined that the removal percentages increased with increasing initial solution pHs. The experiments performed to assess the reusability of synthesized materials gave promising results at low metal ion concentrations.

X-ray photoelectron spectroscopic analyses show that Co^{2+} removal occurs due to fixation on hydroxyl groups at the surface of the shell of iron nanoparticles or via the precipitation of $Co(OH)_2$ at higher concentrations, when the oversaturation conditions are satisfied. On the other hand, Cu^{2+} fixation occurs through the reduction of Cu(II) to Cu(I) in the form of Cu_2O, in addition to metallic copper, Cu^0.

Although more work is still needed to clarify the effects of clay:iron ratios on ion removal capacity and to optimize them in relation with the operating sorption mechanism, the performed studies indicate that kaolinite- and montmorillonite-supported zero-valent iron nanoparticles are promising reactive materials for environmental nanotechnological applications.

REFERENCES

Baird, Colin. 2001. *Environmental Chemistry - Second Edition*. W.H. Freeman and Company.

Blowes, D.W., Ptacek, C.J., Benner, Shawn G., McRae, Che W.T, Bennett, T.A., Puls, R.W. 2000. Treatment of inorganic contaminants using permeable reactive barriers. *Journal of Contaminant Hydrology* 45:123-137.

Braggs, B., Fornasiero, D., Ralston, J., St. Smart, R. 1994. The Effect Of Surface Modification By An Organosilane On The Electrochemical Properties of Kaolinite. *Clays and Clay Minerals* 42(2):123-136.

Chemistry : Periodic Table : iron : standard reduction potentials. 2007. Web of Elements. http://www.webelements.com/webelements/elements/text/Fe/redn.html (accessed Septemer 30, 2007)

Chen, J.P. and Wu, S. 2004. Simultaneous adsorption of copper ions and humic acid onto an activated carbon. *Journal of Colloid and Interface Science* 280:334.

CoulterCounter.com - BET Surface Area & Pore Size Distribution Analysis. 2006. Becman Coulter Inc. http://www.beckmancoulter.com/coultercounter/homepage_tech_bet.jsp (accessed October 11, 2007).

Çelebi, O., Üzüm, Ç., Shahwan, T., Erten, H.N. 2007. A radiotracer study of the adsorption behavior of aqueous Ba^{2+} ions on nanoparticles of zero-valent iron. *Journal of Hazardous Materials* 148:761-767

Da Fonseca, M.G., de Oliveira, M.M., Arakaki, L.N.H., Espinola J.G.P., Airoldi, C. 2005. Natural vermiculite as an exchanger support for heavy cations in aqueous solutions. *Journal of Colloid and Interface Science* 285:50–55.

Demirbas, E. 2003. Adsorption of cobalt(II) ions from aqueous solution onto activated carbon prepared from hazelnut shells. *Adsorpion Science and Technology* 21:951–963.

Ekmekyapar F, Aslan A, Bayhan YK, Cakici, A. 2006. Biosorption of copper(II) by nonliving lichen biomass of Cladonia rangiformis hoffm. *Journal of Hazardous Materials* 137(1):293-298.

El-Dessouky, S.I., El-Sofany, E.A., Daoud, J.A. 2007. Studies on the sorption of praseodymium (III), holmium (III) and cobalt (II) from nitrate medium using TVEX–PHOR resin. *Journal of Hazardous Materials* 143:17-23.

Electron Energy Loss Spectroscopy. 2007. Kyoto University. http://eels.kuicr.kyoto-u.ac.jp/eels.en.html (accessed October 10, 2007).

Evangelou, V.P. 1998. *Environmental Water and Soil Chemistry - Principles and Applications*. New York: John Wiley & Sonc, Inc.

Feng, J., Lim, T.T. 2007. Iron-mediated reduction rates and pathways of halogenated methanes with nanoscale Pd/Fe: Analysis of linear free energy relationship. *Chemosphere* 66:1765–1774.

Feynmans Classic Talk. 2007. Renssealer Polytechnic Institute. http://www.rpi.edu/dept/materials/COURSES/NANO/shaw/Page5.html (accessed Septemer 30, 2007).

Gaarenstroom S.W., Winograd, N. 1977. Initial and Final-State Effects in Esca Spectra Of Cadmium And Silver-Oxides. *Journal of Chemical Physics* 67(8):3500-3506.

Gupta, V.K. and Ali, I. 2000. Utilisation of bagasse fly ash (a sugar industry waste) for the removal of copper and zinc from wastewater. *Separation And Purification Technology* 18 (2):131-140.

He, F. and Zhao, D. 2007. Manipulating the Size and Dispersibility of Zerovalent Iron Nanoparticles by Use of Carboxymethyl Cellulose Stabilizers. *Environmental Science & Technology* 41:6216-6221.

Jaruwong, P., Aumpush, J., Kiattikomol, R. 2005. Uptake of Cationic and Azo Dyes by Montmorillonite in Batch and Column Systems. *Thammasat International Journal of Science and Technology* 10(1):53.

Jenniss, S.W., Katz, S.A., Lynch, R.W. 1997. *Atomic Absorption Spectrometry. in Application of Atomic Spectrometry to Regulatory Compliance Monitoring*. New York: Wiley-VCH, Inc.

Kanel, S.R., Greneche, J., Choi, H. 2006. Arsenic(V) Removal from Groundwater Using Nano Scale Zero-Valent Iron as a Colloidal Reactive Barrier Material. *Environmental Science & Technology* 40:2045-2050.

Kanel, S.R., Manning, B., Charlet, L., Choi, H. 2005. Removal of Arsenic(III) from Groundwater by Nanoscale Zero-Valent Iron. *Environmental Science & Technology* 39:1291-1298.

Konno, H., Nagayama, M. 1980. X-ray Photoelectron-spectra of Hexavalent Iron. *Journal of Electron Spectroscopy and Related Phenomena* 18(4):341-343.

Korea Atomic Energy Research Institute. 2007. http://www.kntc.re.kr/Cyberserver/openlec/nuke(2)/nuclearfeul/nuclearfeul_13/ch13_4.html (accessed October 11, 2007).

Korth, B.D., Keng, P., Shim, I., Bowles, S.E., Tang, C., Kowalewski, T., Nebesny, K.W., Pyun, J. 2006. Polymer-Coated Ferromagnetic Colloids from Well-Defined Macromolecular Surfactants and Assembly into Nanoparticle Chains. *Journal of the American Chemical Society* 128(20):6562 – 6563.

Lawes, G. and James, A.M. 1987. *Scanning Electron Microscopy and X-Ray Microanalysis*. London: John Wiley & Sons.

Li, L., Fan, M., Brown, R.C., van Leeuwen, L. 2006. Synthesis, Properties, and Environmental Applications of Nanoscale Iron-Based Materials: A Review. *Critical Reviews in Environmental Science and Technology* 36:405-431.

Li, X. and Zhang, W. 2006. Iron Nanoparticles: the Core-Shell Structure and Unique Properties for Ni(II) Sequestration. *Langmuir* 22:4638-4642.

Li, X. and Zhang, W. 2007. Sequestration of Metal Cations with Zerovalent Iron NanoparticlessA Study with High Resolution X-ray Photoelectron Spectroscopy (HR-XPS). *Journal of Physical Chemistry C* 111(19):6939-6946.

Li, X., Brown, D.G., Zhang, W. 2007. Stabilization of biosolids with nanoscale zero-valent iron (nZVI). *Journal of Nanoparticle Research* 9:233-243.

Lien, H., Jhuo, Y., Chen, L. 2007. Effect of Heavy Metals on Dechlorination of Carbon Tetrachloride by Iron Nanoparticles. *Environmental Engineering Science* 24(1):21-30.

Liu, Y., Choi, H., Dionysiou, D., Lowry, G.V. 2005a. Trichloroethene Hydrodechlorination in Water by Highly Disordered Monometallic Nanoiron. *Chemistry of Materials* 17:5315-5322.

Liu, Y., Majetich, S.A., Tilton, R.D., Sholl, D.S., Lowry, G.V. 2005b. TCE Dechlorination Rates, Pathways, and Efficiency of Nanoscale Iron Particles with Different Properties. *Environmental Science & Technology* 39:1338-1345.

Manahan, S.E. 1991. *Environmental Chemistry, 5th ed*. Chelsea, MI: Lewis Publishers.

McIntyre, N.S. and Cook, M.G. 1975. X-ray photoelectron studies on some oxides and hydroxides of cobalt, nickel, and copper. *Analytical Chemistry* 47:2208-2213.

McIntyre, N.S., Johnston, D.D., Coatsworth, L.L., Davidson, R.D. and Brown, J.R. 1990. X-ray photoelectron spectroscopic studies of thin film oxides of cobalt and molybdenum. *Surface and. Interface Anaysis* 15:265-272.

Ngo, A.T., Pileni, M. P. 2001. Assemblies of Ferrite Nanocrystals: Partial Orientation of the Easy Magnetic Axes. *Journal of Physical Chemistry B* 105:53-58.

Noubactep, C., Meinrath, G., Dietrich, P., Sauter, M., Merkel, B.J. 2005. „Testing the Suitability of Zerovalent Iron Materials for Reactive Walls. *Environmental Chemistry* 2:71-76.

Nurmi, J.T., Tratnyek, P.G., Sarathy, G., Baer, D.R., Amonette, J.E., Pecher, K., Wang, C., Linehan, J.C., Matson, M.W., Penn, R.L., Driessen, M.D. 2005. Characterization and Properties of Metallic Iron Nanoparticles: Spectroscopy, Electrochemistry, and Kinetics. *Environmental Science & Technology* 39:1221, 1230.

Nuxoll, E.E., Shimotori, T., Arnold, W.A., Cussler, E.L. 2003. Iron Nanoparticles in Reactive Environmental Barriers. AIChE Annual Meeting, Minneapolis, (November 20 2003), Unpublished.

Pagenkopf, G.K. 1978. *Introduction to Natural Water Chemistry.* New York: Marcel Dekker, Inc.

Paparazzo, E. 1987. X-ray photo-emission and Auger spectra of damage induced by Ar^{+}-ion etching at SiO_2 surfaces. *Journal of Physics D: Applied Physics* 20:1091-1094.

Ponder, S.M., Darab, J.G., Mallouk, T.E. 2000. Remediation of Cr(VI) and Pb(II) Aqueous Solutions Using Supported, Nanoscale Zero-valent Iron. *Environmental Science & Technology* 34:2564 – 2569.

Rangsivek, R. and Jekel, M.R. 2005. Removal of dissolved metals by zero-valent iron (ZVI): Kinetics, equilibria, processes and implications for stormwater runoff treatment. *Water Research* 39:4153-4163.

Rengaraj, S. and Moon, S.H. 2002. Kinetics of adsorption of Co(II) removal from water and wastewater by ion exchange resins. *Water Research* 36:1783–1793.

Rock classification. 2007. Seafriends. http://www.seafriends.org.nz/enviro/soil/rocktbl1.htm#claystruct (accessed Septemer 30, 2007).

Shahwan T., 2000. *Radiochemical and Spectroscopic Studies of Cesium, Barium, and Cobalt Sorption on Some Natural Clays*. PhD Thesis submitted to Department of Chemistry and Institute of Engineering and Science, Bilkent University.

Scheinberg, H., 1991. *Copper. in Metals and theirCompounds in the Environment: Occurrence, Analyses and Biological Relevance, edited by E. Merian.* New York: VCH Publishers.

Schrick, B., Blough, J.L., Jones, A.D., Mallouk, T.E. 2002. Hydrodechlorination of Trichloroethylene to Hydrocarbons Using Bimetallic Nickel-Iron Nanoparticles. *Chemistry of Materials* 14:5140-5147.

Shukla, S.R. and Pai, R.S. 2005. Adsorption of Cu(II), Ni(II) and Zn(II) on dye loaded groundnut shells and sawdust. *Separation And Purification Technology*. 43 (1).:1-8.

Skoog, D.A., Holler, F.J., Nieman, T.A. 1998. *Principles of Instrumental Analysis*. USA: Brooks/Cole Thomson Learning.

Smičiklas, I., Dimović, S., Plećaš, I., Mitrić, M. 2006. Removal of Co2+ from aqueous solutions by hydroxyapatite. *Water Research* 40:2267-2274.

Sohn, K., Kang, S.W., Ahn, S.,Woo, M., Yang, S. 2006. Fe(0) Nanoparticles for Nitrate Reduction: Stability, Reactivity, and Transformation. *Environmental Science & Technology* 40:5514-5519.

Strobel, A.S. and Heineman, R.W. 1989. *Chemical Instrumentation: A Systematic Approach.* New York: John Wiley & Sons, Inc.

Sun, Y., Li, X., Cao, J., Zhang, W., Wang, H.P. 2006. Characterization of zero-valent iron nanoparticles. *Advances in Colloid and Interface Science* 120:47-56.

Tan, B.J., Klabunde, K.J., Sherwood, P.M.A. 1991. XPS studies of solvated metal atom dispersed (SMAD) catalysts. Evidence for layered cobalt-manganese particles on alumina and silica. *Journal of American Chemical Society* 113:855-861.

The Transmission Electron Microscope. 2007. Nobel Web AB. http://nobelprize.org/educational_games/physics/microscopes/tem/index.html (accessed October 10, 2007).

Tratnyek, P.G and Johnson, R.L. 2006. Nanotechnologies for environmental cleanup. *Nano Today* 1(2):44-48.

U.S. Department of the Interior, U.S. Geological Survey. 2001. USGS OFR01-041: X-Ray Diffraction Primer. http://pubs.usgs.gov/of/2001/of01-041/htmldocs/xrpd.htm (accessed Septemer 30, 2007).

Van Hullebusch, E.D., Gieteling, J., Zhang, M., Zandvoort, M. H., Daele, W.V., Defrancq, J., Lens, P.N.L. 2006. Cobalt sorption onto anaerobic granular sludge: Isotherm and spatial localization analysis. *Journal of Biotechnology* 121:227-240.

Varanasi, P., Fullana, A., Sidhu, S. 2007. Remediation of PCB contaminated soils using iron nano-particles. *Chemosphere* 66:1031-1038.

Veli, S. and Alyuz, B. 2007. Adsorption of copper and zinc from aqueous solutions by using natural clay *Journal of Hazardous Materials* 149 (1):226-233.

Verbych, S., Bryk, M., Chornokur, G., Fuhr, B. Removal of Copper(II) from Aqueous Solutions by Chitosan Adsorption. *Separation Science and Technology* 40(8):1749 – 1759.

Wagner, C.D. 1975. Chemical shifts of Auger lines, and the Auger parameter. *Faraday Discussions of the Chemical Society* 60:291.

Wagner, C.D., Riggs, W.M., Davis, L.E., Moulder, J.F., Muilenberg, G.E. 1979. *Handbook of X-Ray Photoelectron Spectroscopy, Perkin-Elmer Corporation, Physical Electronics Division*. Minn. 55344: Eden Prairie.

Wang, C. and Zhang, W. 1997. Synthesizing Nanoscale Iron Particles for Rapid and Complete Dechlorination of TCE and PCBs. *Environmental Science & Technology* 31(7):2154-2156.

Wang, W., Jin, Z., Li, T., Zhang, H., Gao, S. 2006a. Preparation of spherical iron nanoclusters in ethanol–water solution for nitrate removal. *Chemosphere* 65:1396-1404

Wang, X., Wang, J., Sun, C 2006b. Removal of Copper(II) Ions from Aqueous Solutions Using Natural Kaolinite. *Adsorption Science & Technology* 24(6):517:530.

Wikipedia contributors, "Copper". 2007a. Wikipedia, The Free Encyclopedia. http://en.wikipedia.org/wiki/Copper (accessed Septemer 29, 2007).

Wikipedia contributors, "Cobalt". 2007b. Wikipedia, The Free Encyclopedia. http://en.wikipedia.org/wiki/ Cobalt (accessed Septemer 29, 2007).

Wikipedia contributors, "Iron". 2007c. Wikipedia, The Free Encyclopedia. http://en.wikipedia.org/wiki/Iron (accessed Septemer 30, 2007).

Wikipedia contributors, "Montmorillonite". 2007d. Wikipedia, The Free Encyclopedia. http://en.wikipedia.org/wiki/ Montmorillonite (accessed Septemer 29, 2007).

Wikipedia contributors, "Transmission Electron Microscopy". 2007e. Wikipedia, The Free Encyclopedia. http://en.wikipedia.org/wiki/Transmission_electron_microscopy (accessed October 10, 2007).

Zhang, W. 2003. Nanoscale iron particles for environmental remediation: An overview. *Journal of Nanoparticle Research* 5:323-332.

Zhang W and Elliot, D.W. 2006. Applications of Iron Nanoparticles for Groundwater Remediation. *REMEDIATION* Spring 2006:7-21.

Zhang, H., Jin, Z., Han, L., Qin, C. 2006. Synthesis of nanoscale zero-valent iron supported on exfoliated graphite for removal of nitrate. *Transactions of Nonferrous Metals Society of China* 16:345-349.

Zhu, B., Lim, T., Feng, J. 2006. Reductive dechlorination of 1,2,4-trichlorobenzene with palladized nanoscale Fe0 particles supported on chitosan and silica. *Chemosphere* 65:1137-1145.